Influence of elastic-viscoplastic behaviour on the filling efficiency of amorphous thermoplastic polymer during the micro hot embossing process

Faleh Rabhi, Gang Cheng, Thierry Barriere, Nourredine Aït Hocine

Elsevier Editorial System(tm) for Journal of Manufacturing Processes

Manuscript Draft

Manuscript Number: SMEJMP-D-20-00801R1

Title: Influence of elastic-viscoplastic behaviour on the filling efficiency of amorphous thermoplastic polymer during the micro hot embossing process

Article Type: Full Length Article

Keywords: micro hot embossing process; poly-methyl methacrylate; elastic-viscoplastic constitutive law; numerical simulation.

Corresponding Author: Dr. Gang Cheng, Ph.D.

Corresponding Author's Institution: INSA Centre Val de Loire

First Author: Faleh Rabhi

Order of Authors: Faleh Rabhi; Gang Cheng, Ph.D.; Thierry Barrière; Nourredine Aït Hocine

Abstract: An unsolved issue in simulating the hot embossing of polymers is modelling the unfilled structured mould. This is because the constitutive law of such polymers has not been adequately determined, especially at the microscale or smaller. The present study investigated the influence of the elastic-viscoplastic behaviour on the filling efficiency of an amorphous polymer during the micro hot embossing process. Constitutive equations based on the two-layer viscoplastic model were used to simulate the hot embossing process. The micro-cavity of the mould was completely filled by the polymer, and the elastic, viscous, and plastic behaviours were considered simultaneously in the simulation. Compression tests were performed to identify the model parameter values for poly-methyl methacrylate. A numerical simulation was performed to analyse the contributions of the polymer's elastic, viscous, and plastic behaviours. The unfilled area in the micro-cavity was evaluated after a displacement of 0.2 mm was applied to the mould. This was used as an indicator to compare the mould filling efficiency with those of the elastoplastic and elastic-viscoplastic constitutive models. The analysis led to the selection of an optimal elastic-viscoplastic model to completely fill the micro-cavity, which was consistent with the experimental results.

Suggested Reviewers:

Opposed Reviewers:

[Date of submission: 06/08/2020]

S. Kapoor
Editor-in-Chief
Journal of Manufacturing Processes

Dear Editor:

We/I wish to re-submit the manuscript titled “Influence of elastic-viscoplastic behaviour on the filling efficiency of amorphous thermoplastic polymer during the micro hot embossing process.” The manuscript ID is No.: SMEJMP-D-20-00801.

We thank you and the reviewers for your thoughtful suggestions and insights. The manuscript has benefited from these insightful suggestions. I look forward to working with you and the reviewers to move this manuscript closer to publication in the *Journal of Manufacturing Processes*.

The manuscript has been rechecked and the necessary changes have been made in accordance with the reviewers’ suggestions. The responses to all comments have been prepared and attached herewith/given below.

Thank you for your consideration. I look forward to hearing from you.

Sincerely,

Gang Cheng
INSA CVL
Université Tours, Université Orléans, LaMé, 3 rue de la Chocolaterie, CS 23410, 41034 Blois Cedex, France
Tel: +33 2 54 55 86 96
gang.cheng@insa-cvl.fr

COMMENTS FOR THE AUTHOR:

Reviewer #2: The article is of a certain interest, but it requires major revision before publication.

Thank you for your valuable comments, suggestions, and remarks. All of your remarks and comments were taken into account in revising the paper. Some sentences were added in the manuscript in red.

1. In my opinion, the last paragraph of the first section "Introduction" is unnecessary. Please just point out the main studying contents of this paper here.

Response: The last paragraph of Section “Introduction” was replaced by a new paragraph pointing out the main contents of this study, as shown in the last paragraph of Section 1.

2. Please list the boundary conditions for the numerical simulations in this paper.

Response: As suggested by the reviewer, the whole boundary conditions were listed in the revised version of the manuscript (see the 3rd paragraph of Section 4).

3. Provide more information about the equipment, mold, and material (brand name et al.) used for the verification experiments.

Response: More information about the equipment, mould and PMMA material are now given in the text in Section 3.1 and 5.3.

4. The Conclusion section should be reorganized. Only retain the real conclusion of this research is enough.

Response: The conclusion (Section 6) was rewritten to point out only the main results.

5. There is no Graphical Abstract for this manuscript.

Response: A graphical abstract was added in the revised version of the paper.

Reviewer #5: The paper entitled “Influence of elastic-viscoplastic behaviour on the filling efficiency of amorphous thermoplastic polymer during the micro hot embossing process” is within the journal scope and is up-to-date in terms of presented investigations.

The paper is three models dedicated polymers. The models were investigated for the selected embossing process.

The problem is well defined and the paper structure is proper.

Thank you for your valuable comments, suggestions, and remarks. We added some new sentences to the revised version of the paper to better illustrate scientific aspects. All of your remarks and comments were taken into account in revising the paper.

Detailed comments are listed below.

1. Page 9. For identification of parameters of the two-branches models inverse approach was applied. The Authors should add some more details of that identification.

Response: As suggested by the reviewer, more details were added regarding the identification of parameters of the two-layer model. In fact, in the two-layer viscoplastic model, four essential parameters (f, m, A and n_2) need to be identified. True stress-strain curves were obtained from compression tests carried out on the studied material.

f is the ratio of the elastic modulus of the viscoelastic branch to the total modulus. Some more details concerning the identification of this parameter were given in Section 3.2.

m is time-hardening power law parameter. When the strain rate remained constant, this parameter was set to zero, as described in the text between Eq. 3 and 4.

A and n_2 are Norton constants, identified from the true viscous stress and strain curves obtained in stress relaxation tests, as described in the text before Table 2.

2. The authors wrote that the numerical simulations and the new rheological equation was implemented in Abaqus software. Could you add some more information about this part of the work? Besides material characteristic what about the boundary conditions, mesh description – elements type, total time of simulation, convergence of the solution and so on.

Response:

The numerical geometry model was created by the authors, but the two-layer viscoplastic model was embedded in Abaqus. The model was originally used for the mechanical behaviour of metals at high temperature. The authors adapted this model to the behaviour of the studied thermoplastic polymer. All the material parameters of the model were identified based on the experimental tests effectuated by the authors. Some details were added in the manuscript in the beginning of Section 2.

More details concerning the boundary conditions, mesh description including elements type, total time of simulation, and convergence of the solution were given in the last paragraph of Section 4, in the revised version of the manuscript.

3. Figs. from 7 to 12. Could you present the results with one scale (for each figure one scale)? It helps to analyse the results.

Response:

Thank you for your suggestion but we propose to show the maximal and minimal values of stress and strain, in Figs. from 7 to 12, to analyse the simulation results. These presentations

are in accordance with the explanations given in the text, and they will certainly help the readers to understand the results better. However, if the reviewer still wishes the results to be presented with one scale, the author could do it.

4. Section 5.2. Sensitivity of the model with respect to the parameter f. Four values were analysed. How were they selected? What about the remaining parameters? Were they fixed? Please clarify.

Response:

These values of f were selected arbitrarily from 0 to 1 and all the other material parameters were fixed. More explanations were added in the second paragraph of Section 5.2, in the revised version of the manuscript.

5. Fig. 13. The model validation. The quality of this figure is poor. It is hard understand how the model was validated. Could you introduce some quality measure to compare the experimental results to numerical ones? Now it is only qualitatively comparison and validation, as I understood.

Response:

The quality of the figure was improved, and a detailed image of the microfluidic feature was given to explain the experimental validation better, as shown in Fig. 13 of the revised version of the manuscript. A cross-sectional profile of the replicated PMMA microfluidic device was added in this figure to show the measurement of the height, in order to validate the numerical results. More explanations were given in Section 5.3.

6. In the conclusions is written, that the most important parameter is f. But I did not find in the paper any analysis of all parameters which would allow for such a statement. Please justify it. The paper is interesting but requires some revision.

Response:

The conclusion was rewritten to point out only the main results. f was the ratio of the elastic modulus of the viscoelastic branch to the total modulus. It is the only parameter among the four parameters, concerning the viscoelastic properties of the material, which was considered to be essential to the filling ratio of the micro die cavity. Thus, the sensitivity analysis of this parameter was provided in Section 5.2. The authors wanted to know how f affected the filling efficiency of the micro die cavity in hot embossing process. The results showed that the micro-cavity was filled more when f was close to 1, which indicates that increasing the elasticity in the viscoelastic branch can improve the filling efficiency of the polymer flow during the micro hot embossing process.

Graphical Abstract (for review)

Micro hot embossing process of the polymers with high replication accuracy

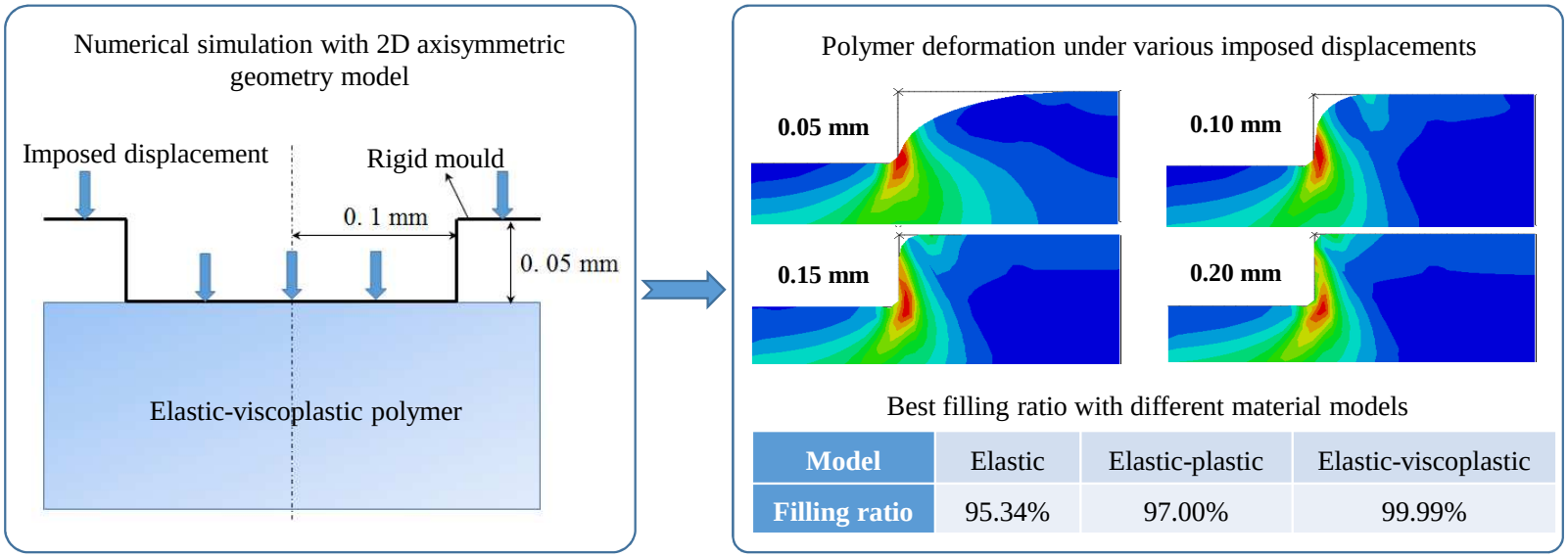

Best filling ratio with different material models

Model	Elastic	Elastic-plastic	Elastic-viscoplastic
Filling ratio	95.34%	97.00%	99.99%

Highlights

Two-layer viscoplastic model was developed for the micro hot embossing process

Elastic/elastoplastic/elastic-viscoplastic behaviours of the polymer were considered

Experiments were performed to validate the simulation results

Elastic-viscoplastic behaviour is needed to accurately model the polymer

Influence of elastic-viscoplastic behaviour on the filling efficiency of amorphous thermoplastic polymer during the micro hot embossing process

F. Rabhi[a,b], G. Cheng[b,*], T. Barriere[a], N. Aït Hocine[b]

[a] Université Bourgogne Franche-Comté, FEMTO-ST Institute, CNRS/UFC/ENSMM/UTBM, Department of Applied Mechanics, 25000 Besançon, France

[b] INSA CVL, Université Tours, Université Orléans, LaMé, 3 rue de la Chocolaterie, CS 23410, 41034 Blois Cedex, France

* Corresponding author: gang.cheng@insa-cvl.fr

Abstract

An unsolved issue in simulating the hot embossing of polymers is modelling the unfilled structured mould. This is because the constitutive law of such polymers has not been adequately determined, especially at the microscale or smaller. The present study investigated the influence of the elastic-viscoplastic behaviour on the filling efficiency of an amorphous polymer during the micro hot embossing process. Constitutive equations based on the two-layer viscoplastic model were used to simulate the hot embossing process. The micro-cavity of the mould was completely filled by the polymer, and the elastic, viscous, and plastic behaviours were considered simultaneously in the simulation. Compression tests were performed to identify the model parameter values for poly-methyl methacrylate. A numerical simulation was performed to analyse the contributions of the polymer's elastic, viscous, and plastic behaviours. The unfilled area in the micro-cavity was evaluated after a displacement of 0.2 mm was applied to the mould. This was used as an indicator to compare the mould filling efficiency with those of the elastoplastic and elastic-viscoplastic constitutive models. The analysis led to the selection of an optimal elastic-viscoplastic model to completely fill the micro-cavity, which was consistent with the experimental results.

Keywords: micro hot embossing process, poly-methyl methacrylate, elastic-viscoplastic constitutive law, numerical simulation.

Nomenclature

A, n_2	Norton constants
D	Final diameter
D_0	Initial diameter
d	Mould displacement
d_{max}	Maximum mould displacement
E	Elastic modulus
F^c	Compressive force
f	Proportion of elasticity in the viscoelastic branch to total elasticity
H	Final height
H_0	Initial height
H'	Power law hardening
K	Total elastic modulus
K_p	Elastic modulus in the elastoplastic branch
K_v	Elastic modulus in the viscoelastic branch
m	Time-hardening power law parameter
n_1	Work hardening exponent
$PMMA$	Poly-methyl methacrylate
S	Final cross-sectional area
S_0	Initial cross-sectional area
T_g	Glass transition temperature
t	Testing time
$\dot{\varepsilon}$	Strain rate
ε_v^{el}	Elastic strain of the viscoelastic branch
ε_p^{el}	Elastic strain in the elastoplastic branch
ε^{el}	Total elastic strain
ε^{pl}	Plastic strain
ε^{v}	Viscous strain
ε	Total strain
η	Viscosity
σ	Total stress
σ_p	Plastic stress
σ_γ	Initial yield stress
σ_v	Viscous stress
ϑ	Displacement rate
υ	Poisson's ratio

1. Introduction

Poly-methyl methacrylate (PMMA) is desirable for many practical engineering applications, especially in micro-optics and microfluidic devices. It is commonly used as an embossing substrate. Microscale fluidic composites have appeared with the development of microelectronics and are widely employed in the fields of chemistry, biology, and diagnostics. They provide many advantages compared to conventional macroscale devices, such as reduced reagent consumption, more portable instrumentation, and reduced analysis time. Many manufacturing methods are available for polymer materials, such as injection moulding, compression, and extrusion moulding. These processes must be optimised to improve the functional properties and quality of the final components. Trotta et al. [1] developed an innovative metallic tool for the micro injection moulding process to achieve the mass-production of polymer-based microfluidic devices. The microfeatures in the mould tool were well replicated by the amorphous thermoplastic polymer. Sucularli et al. [2] used an ultrasonic embossing process to elaborate the microfluidic devices with a thermoplastic substrate. They showed that the friction between the polymer substrate and the mould improved the filling efficiency. There is wide interest in the polymer hot embossing process, especially for manufacturing microscale components or smaller.

Hot embossing can replicate polymer microstructures with a high level of quality. During this process, the polymer plate is compressed at a temperature above the polymer's glass transition temperature (T_g). Compared to the conventional injection moulding process, it has significant advantages in being able to realise a high aspect ratio and large replication area with micro- and nanoscale geometries. Lin et al. [3] investigated the influence of pressure parameters on hot embossing in the cooling stage. They studied the evolution of cooling shrinkage through analytical models and experiments to realise accurate components. Their results indicated that a higher embossing pressure results in more uniform shrinkage during cooling in the elastic

deformation state. Chien and Yu [4] used three innovative methods for micro mould manufacturing to realise 3D layer structures with PMMA. They combined photolithography and electroplating to form metal patterns with silicon and glass wafers as the mould. Cheng et al. [5] successfully employed hot embossing with an innovative injection-moulding press and elastomeric mould to manufacture microfluidic systems of PMMA slightly above its T_g. Huang and Lu [6] performed nanoindentation measurements on PMMA below T_g and identified the behaviour of two independent viscoelastic functions at the sub-micron scale. Cheng et al. [7] investigated the influence of a polymer's thermomechanical properties and the effects of processing parameters on the optimisation of the micro-manufacturing process to realise advanced 2D PMMA devices. They were able to manufacture an excellent device without defects and with low plastic deformation at a high technical level. Wang et al. [8] considered the polymer recovery properties and optimised the associated processing time and forming temperature parameters of the micro hot embossing process in experiments and obtained a filled state with high accuracy and efficiency. He et al. [9] fabricated successfully a super hydrophobic polymer channel by using the hot embossing process. Hot embossing exhibited high accuracy and high efficiency in the manufacturing process of polymeric materials. Hu et al. [10] developed a non-isothermal polymer hot embossing process to study micro-prisms and presented an experimental temperature field for hot embossing tools and polymer specimens. With the optimised parameters, they obtained a hot-embossed surface roughness of 10–30 nm and a relevant correlation between the experimental data and analytical micro-formations.

The weakness of material behaviour modelling and associated simulations has limited future development dedicated to the micro hot embossing process. Dorenzi and Nied [11] used nonlinear elastic behaviour coupled with incompressible conditions to simulate the hot embossing process for a 2D polymeric membrane specimen. They developed a numerical

algorithm to predict the mould temperature field. Their approach was limited because of the uncertain heat transfer coefficient for various thermal mechanisms.

Many experiments have been performed to analyse the behaviour and identify the properties of amorphous polymers in the temperature range below T_g. Cheng et al. [12] used both experiments and models to investigate the viscoelastic behaviour of amorphous PMMA during the micro hot embossing process. Wang et al. [13] performed uniaxial compression tests to analyse the rate- and temperature-dependent mechanical behaviours of polycarbonate at room temperature. Covezzi et al. [14] developed an innovative homogenisation method to analyse the nonuniform distribution of the inelastic strain in viscoplastic composite materials. Fewer history variables were employed in the model, and the accuracy and effectiveness of the proposed technique were confirmed by a comparison with micromechanical analyses. Gudimetla and Doghri [15] proposed a coupled viscoelastic and viscoplastic model to analyse the mechanical response of an amorphous polymer under static and cyclic loadings. Holopainen and Barriere [16] modelled the behaviour of amorphous glassy polymers by using viscoelastic-viscoplastic constitutive laws based on experimental tests. Some viscoelastic, viscoplastic, and elastic-viscoplastic models have been developed to explore the physical constitutive behaviour laws of amorphous polymers. Sorini et al. [17] conducted uniaxial tension, uniaxial compression, and shear tests with a representative epoxy over a range of strain rates and temperatures to investigate the viscoplastic behaviour of the material. A constitutive viscoplastic polymer model was proposed to analyse the effects of adiabatic heating and thermal softening on the response of the polymer matrix composites. Above T_g, deforming a polymer becomes progressively easier, which helps in fully filling micro-cavities. However, few studies have considered the complex material behaviour of polymers, especially PMMA, slightly above T_g. PMMA exhibits elastic-viscoplastic behaviour in this temperature range, and the physical modelling of such behaviour is a real scientific challenge.

Physically modelling amorphous polymer behaviour has become an important scientific issue in the past few years, especially because of the complex behaviour close to T_g. Material models show excellent flexibility and are sensitive to different strain rates. Cheng et al. [12] used a generalised Maxwell model with ten branches for the constitutive law. They developed this model according to the true stress–true strain curve obtained for PMMA in dynamic compression tests above T_g. Their model indicated that plastic deformation occurs above T_g, even though it decreases with increasing temperature. In this case, they only considered the viscoelastic constitutive behaviour for the hot embossing simulation, which limited the modelling accuracy of the polymer behaviour. Farias et al. [18] proposed a variational framework to model PMMA behaviour under finite strains. They used a two-branch viscoelastic Maxwell model comprising a biexponential flow resistance branch and constant resistance branch to capture the unloading history of PMMA close to T_g. A 3D simulation of a standard tensile test with heterogeneous material illustrated the capabilities of the proposed framework with finite element software. Wang et al. [19] proposed a thermodynamics-based constitutive model to analyse the influence of the intrachain stress on polymer deformation and processing. The developed model is suitable for predicting creep, relaxation, and recovery, which is convenient for modelling the viscoelastic and viscoplastic behaviour of amorphous glassy polymers with large deformations. Mahjoubi et al. [20] proposed a physics-based constitutive model to describe the viscoplastic and hyperelastic behaviours of glassy materials. The proposed model better describes the anisotropic effects due to molecular ordering during plastic yielding for large strains and a wide temperature range. Niyonzima et al. [21] developed a thermos-mechanical constitutive model coupled with an electromagnetic field to describe the large deformation of the shape memory polymers. The numerical simulation of the deployment of the polymer stent in a vein of an arm was successfully achieved with the finite element method. Cheng and Barriere [22] simulated the filling stage

simulation of the hot embossing process using only an elastoplastic constitutive model. Therefore, they could not capture the viscous deformation of the polymer flow during embossing.

The two-layer viscoplastic behaviour law was initially developed for metals and comprises parallel elastoplastic and viscoelastic branches. Charkaluk et al. [23] proposed an elastic-viscoplastic constitutive law with a two-layer model under thermomechanical loading for cast-iron exhaust manifolds. Leen et al. [24] developed a two-layer viscoplastic model to represent the behaviour of material with a high nickel-chromium content. This model includes both the creep and isotropic-kinematic plasticity and was embedded in Abaqus® software. It was applied to modelling the high-temperature deformation of metals in the case of time-dependent behaviour or plasticity. Berezvai and Kossa [25] adapted two-layer models to describe the behaviour of polymer thermoplastic foam during the thermoforming process. Abdel-Wahab et al. [26] investigated the elastic, viscous, and plastic properties of PMMA at large strains with a two-layer viscoplastic model based on experimental data from different mechanical tests under various loading conditions below T_g. The two-layer viscoplastic model showed better agreement with the experimental results than an elastoplastic model.

The influence of elastic, plastic, and viscous behaviours on the constitutive model for the filling efficiency of the micro hot embossing process has not been fully investigated in the existing literature. In this study, an original method was developed for identifying the filling efficiency of PMMA during the micro hot embossing process considering its elasticity, viscosity, and plasticity. The mechanical properties of PMMA were characterised through a mechanical compression test at 20 °C above T_g (108 °C). The constitutive equations of the two-layer viscoplastic model were retained to describe the physical properties of PMMA. The sensitivity of the viscoplastic model parameters was analysed to verify its effectiveness. A 2D axisymmetric problem was formulated with Abaqus® software. The von Mises stress,

effective plastic strain, and vertical displacement distributions were calculated for the manufacture of microfluidic components from a PMMA plate during the hot embossing process. The numerical results were consistent with the experimental results when a complete behaviour law including elastic, plastic, and viscous behaviours was applied. The proposed two-layer viscoplastic model is suitable and efficient for the numerical simulation of the micro hot embossing process. It can be used to optimise the manufacturing process of polymers at temperatures above T_g.

In this paper, the two-layer viscoplastic model was used to describe the elastic-viscoplastic behaviours of a polymer. The numerical simulation of the filling stage of the micro hot embossing process was achieved, and its accuracy was validated by the experimental results. The sensitivity of the parameter in the model was analysed and the model showed great potential for the numerical simulation of manufacturing processes with polymers.

2. Description of the two-layer viscoplastic model

The two-layer viscoplastic model is embedded in the material database of the Abaqus® software. This model was originally used to describe the viscous and plastic behaviours of metals at high temperature. In this research, the model was adapted to describe the behaviour of the studied material, a PMMA. All the material parameters of the model were identified based on the experimental tests (See Section 3.2).

Fig. 1 shows an ideal two-layer model representing the associated effects of rate-independent and rate-dependent behaviours corresponding to the viscoelastic and elastoplastic branches, respectively. The first layer describes the permanent deformation after a load is applied, and the second layer describes the permanent strain on the material under the load over time. The elastoplastic branch is based on the von Mises yield criterion, and the viscoelastic branch is based on the Norton-Hoff power law.

The model has an elastoplastic branch with the first part representing a Maxwell model to describe the viscoelastic properties, where $m = 0$ for steady-state creep and η is related to the viscosity. The second part of the model includes the elastic modulus of the elastoplastic branch K_p and elastic modulus of the viscoelastic branch K_v. In the third part, σ_γ is the initial yield stress, H' is the hardening parameter, and A and n_2 represent the Norton-Hoff law (creep strain rate = $A\sigma^{n_2}$). The inverse identification strategy was used to optimise the different model parameters.

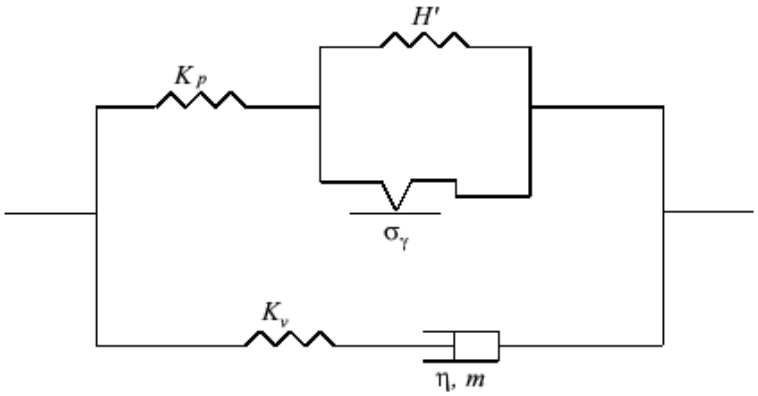

Fig. 1. One-dimensional idealisation of the two-layer viscoplastic model.

The two-layer viscoplastic model considers the elastic, plastic, and viscous deformations of a material and was implemented in the Abaqus® software. The elasticity is defined by the linear isotropic elastic part (Fig. 1). f is the proportion of elasticity in the viscoelastic branch to the total elasticity. The total modulus is defined as $K = K_p + K_v$. f is defined as follows:

$$\begin{cases} f = \frac{K_v}{K_p + K_v} \\ K_v = K - K_p \\ f = \frac{K - K_p}{K} \end{cases} \quad (1)$$

The total stress is defined by adding the viscous stress σ_v in the viscoelastic branch and stress σ_p in the elastoplastic branch. For the elastoplastic constitutive behaviour, the true stress–true strain relationship is given by

$$\sigma_p = \begin{cases} K_p \times \varepsilon \; if \; \sigma_p \leq \sigma_\gamma \\ H' \times \varepsilon^{n_1} \; if \; \sigma_p \geq \sigma_\gamma \end{cases}, \tag{2}$$

where ε is the total strain, σ_γ is the initial yield stress, and n_1 is the work hardening exponent. The coefficient H' can be expressed as

$$H' \times \varepsilon^{n_1} = \frac{\sigma_\gamma}{\varepsilon_y^{n_1}}(\varepsilon_y + \varepsilon_p)^{n_1} = \sigma_\gamma(1 + \frac{\varepsilon_p}{\varepsilon_y})^{n_1} = \sigma_\gamma(1 + \frac{K_p}{\sigma_\gamma}\varepsilon_p)^{n_1}, \tag{3}$$

where ε_y is the strain at the initial yield stress σ_γ and ε_p is the plastic strain.

A time-hardening power law was used for the viscous behaviour by setting $m = 0$; this means that the viscous strain rate $\dot{\varepsilon}$ is independent of time:

$$\sigma_v = A^{-\frac{1}{n_2}}\dot{\varepsilon}^{\frac{1}{n_2}} \tag{4}$$

$$\dot{\varepsilon} = A\sigma_v^{n_2}t^m, \tag{5}$$

where t represents the testing time.

The viscous and plastic properties are independent, and the total stress σ is given by

$$\sigma = \sigma_p + \sigma_v \tag{6}$$

The elastic strain is divided into a viscoelastic part ε_v^{el} and elastoplastic part ε_p^{el}:

$$\varepsilon^{el} = f\varepsilon_v^{el} + (1 - f)\varepsilon_p^{el} \tag{7}$$

The total strain includes the elastic and plastic strains in the elastoplastic branch ε^{pl} and the viscous strain in the viscoelastic branch ε^v:

$$\varepsilon = \varepsilon^{el} + f\varepsilon^v + (1 - f)\varepsilon^{pl} \tag{8}$$

3. Characterisation of the viscoplastic behaviour of a polymer

Uniaxial compression tests were performed to identify the material parameters of the viscoplastic constitutive behaviour in the temperature range for the hot embossing process.

3.1. Description of the uniaxial compression test

The thermoplastic polymer PMMA (Plexiglas® 8N) was used in this study. A cylindrical specimen with a length and diameter of 18 and 10 mm, respectively, was inserted between two metal plates in an oven (Fig. 2). The compression test was performed at $T_g + 20$ °C. The fixed lower metal plate was connected to a force load sensor. The accuracy of the oven temperature was 1 °C. The PMMA compression specimens were heated to anneal for 1 h at the testing temperature to release residual stresses due to injection replication. The mechanical tests were repeated several times on similar specimens with the same constant true strain rate at $T_g + 20$ °C.

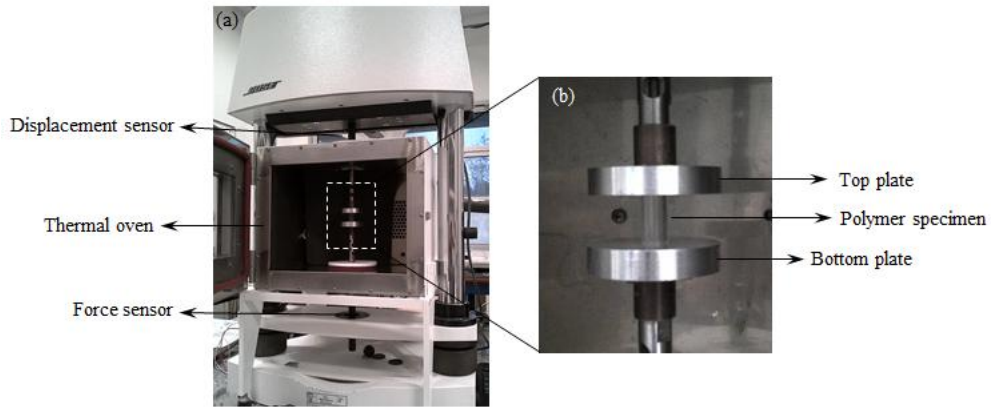

Fig. 2. Experimental setup for mechanical tests (Bose® Electro Force® instrument): (a) overview of the equipment and (b) magnified view of the specimen.

The volume of the PMMA cylindrical specimen was assumed to be constant. The true stress–true strain constitutive law was determined by considering that the specimen remained cylindrical in shape before and after compression.

H_0, D_0, S_0 represented the initial height, diameter, and cross-sectional area, respectively, of the standard specimen. During the compression test, these dimensions became H, D, and S,

respectively. The difference between H and H_0 was measured with a mechanical extensometer (Fig. 3). The PMMA true strain and true stress were calculated as follows:

$$\varepsilon = \ln(\frac{H_0}{H}) \tag{9}$$

$$\sigma = \frac{F^c}{S} = \frac{F^c H}{S_0 H_0}, \tag{10}$$

where F^c is the compressive force.

The strain rate is given by

$$\dot{\varepsilon} = \frac{d\varepsilon}{dt} = \frac{\vartheta}{H_0 - \vartheta t}, \tag{11}$$

where ϑ is the specimen displacement rate.

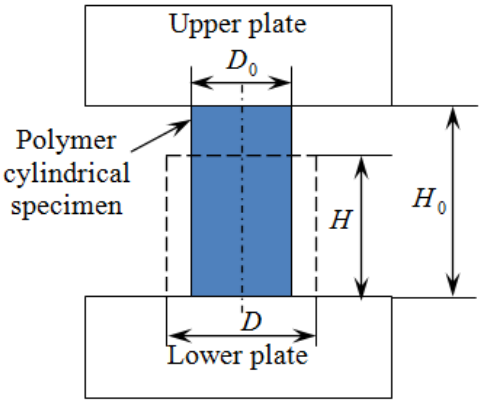

Fig. 3. Schematic of the uniaxial mechanical test with a specimen.

3.2. Identification of the two-layer viscoplastic material parameters

The parameters of the constitutive law were identified from compression tests. One of the most important parameters of the model was f (Eq. (1)), which corresponded to the ratio of the elastic modulus K_v of the viscoelastic branch to the total modulus K (Fig. 1). The total elastic modulus K was the sum of the elastic modulus K_p of the elastoplastic branch and elastic modulus K_v of the viscoelastic branch. The compression tests with a constant and small strain rate 0.01 s^{-1} were carried out at $T_g + 20$ °C [22]. Based on the obtained PMMA true

stress-strain curves, K_p was determined using a linear regression fitting in the true strain range of 0.0005 to 0.0025. The total modulus K was obtained from the stress relaxation tests of PMMA at a high strain rate. In fact, the PMMA specimens were compressed to different strain levels, which were kept constant and the true stress was measured. For each stain level, curves of the relaxation stress vs. time were drawn and the value of K was identified. The average value of K at different strain levels was calculated to ensure the measurement accuracy. The parameter f was calculated with Eq. (1). The values of K_p, K, and f are summarised in Table 1.

Table 1. Two-layer viscoplastic model parameters of PMMA at $T_g + 20$ °C.

Parameter	Value
K_p (MPa)	3.61
K (MPa)	33.38
f	0.89
A (Pa)$^{-n_2}$	6.63×10^{-6}
n_2	0.88
m	0
υ	0.4

The plastic constitutive parameters were identified from the true stress–true strain curve at a constant strain rate. Fig. 4 shows the obtained curve at a strain rate of 0.03 s^{-1}. The yield peak appeared at a true strain of 0.02, and the true yield stress was approximately equal to 0.6 MPa. The remaining deformation was revealed after total unloading of the specimen, which suggests that the tested PMMA had plastic behaviour above T_g. Based on the stress-strain

curve of the compression behaviour at $T_g + 20$ °C, the plastic strains were identified at different stresses, as given in Table 2.

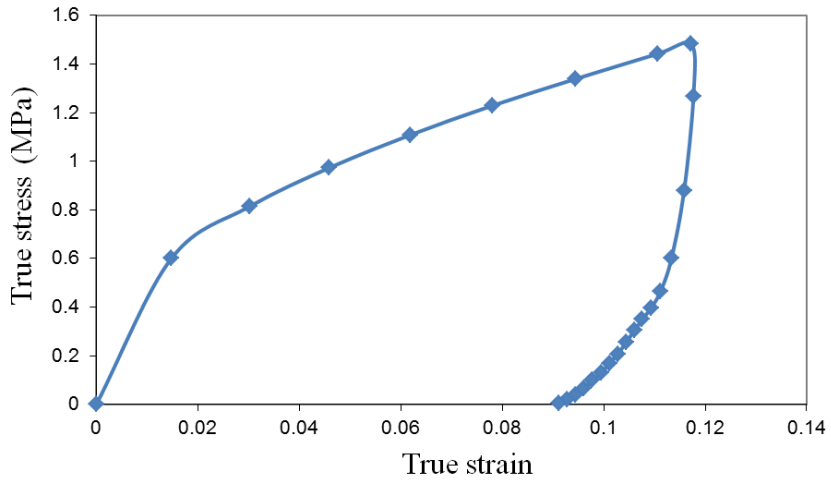

Fig. 4. Stress-strain curve for the compression behaviour of PMMA at $T_g + 20$ °C.

Table 2. Plastic strain of PMMA at $T_g + 20$ °C.

σ (MPa)	ε^{pl}
0.5 ± 0.0001	0 ± 0.0005
0.8 ± 0.0001	0.01 ± 0.0005
1.1 ± 0.0001	0.04 ± 0.0005
1.4 ± 0.0001	0.08 ± 0.0005

The viscoelastic parameters were obtained from the stress relaxation of PMMA at different strain levels and $T_g + 20$ °C with the same method previously used by Cheng and Barriere [22]. The stress rate was calculated by differentiating the relaxation stress over time with the same method used by Alipour Skandani and Al-Haik [27]. The least-squares method was used to determine the total elastic modulus according to the experimental stress-strain curves.

The true stress was obtained for different strain levels in the stress relaxation tests. For each strain level, the curves of the viscous stress vs. strain were drawn to identify A and n_2. Poisson's ratio was considered to be constant for PMMA as determined by Nguyen-Thanh et al. [28]. The parameter values of the developed model are summarised in Table 1.

4. Numerical simulation method

The filling stage of the hot embossing process with amorphous PMMA was simulated while considering the viscoplastic behaviour. Fig. 5 shows a flowchart for integrating the two-layer viscoplastic model in the numerical simulation. The elastoplastic and viscoelastic parameters were identified from the compression tests with PMMA. The value of f was set from 0.2 to 0.8 to investigate the sensitivity of the numerical modelling of the hot embossing process. A 2D axisymmetric model was used to obtain the distributions of the von Mises stress and effective plastic strain in the polymer substrate.

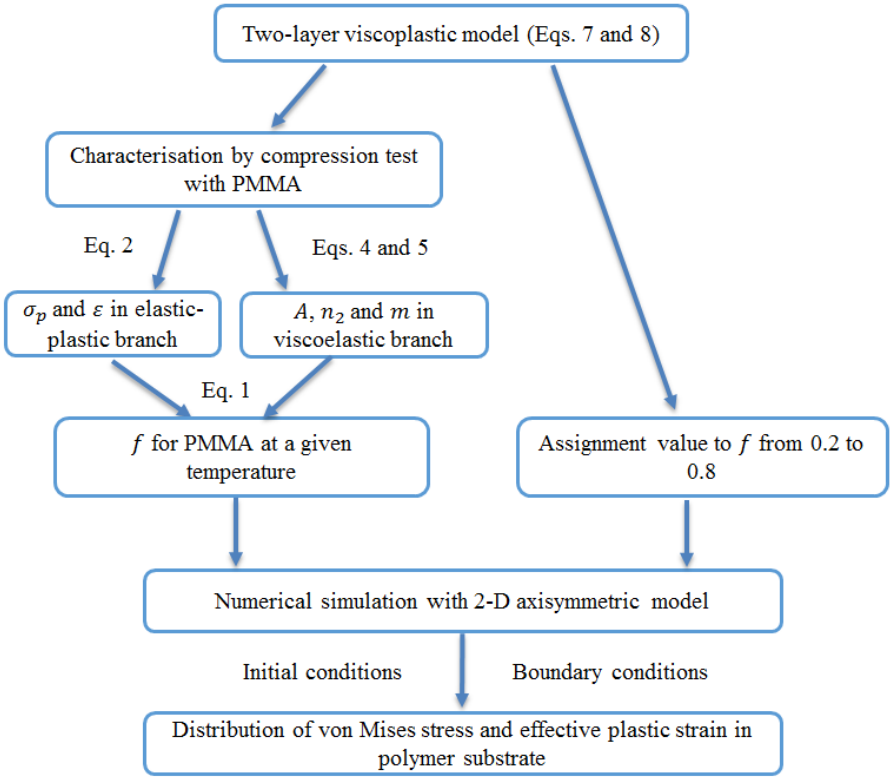

Fig. 5. Flowchart for integration of the two-layer viscoplastic model in the numerical simulation.

The aim of the simulation was to gain an insight into the microscale effects of the mechanical behaviour of the material considering the viscosity and plasticity on the filling stage. The 2D axisymmetric model was used in the Abaqus® simulation software to analyse the circular device (Fig. 6) based on the geometric axisymmetry of the circular cavity at the microscale. A PMMA plate specimen was inserted under the die cavity mould (Fig. 6). The mould compressed the polymer substrate that flowed into the micro-cavity during the embossing process. The cylindrical mould had a radius of 0.1 mm and height of 0.05 mm. The PMMA plate specimen was 1 mm thick. The geometries of both the mould die cavity and plate specimen were considered in the numerical simulation through the use of the 2D axisymmetric geometry model in the Abaqus® software.

Fig. 6 shows the 2D axisymmetric geometry model representing the mould and the polymer. The numerical strain was zero in the mould, which was considered as a rigid body, during the embossing process simulations. The plate specimen was considered to be a deformable solid, whose deformation was described by the material behaviour law. The bottom surface of the mould was in contact with the top surface of the polymer specimen at the beginning of the simulation. A constant vertical displacement was set on the top surface of the mould. The vertical displacement of the bottom surface of the plate specimen was set to 0. The plate specimen was compressed and pushed into the micro-cavity with a height of 0.05 mm, as shown in Fig. 6. Different imposed displacements were applied on the mould. Free triangular and quadratic meshing elements were chosen for the modelling. Several mesh conditions, including mesh size, number, and distribution were applied. The configuration of the mesh condition, ensuring the convergence of the calculations in reasonable time and preserving

calculation accuracy, was 3320 elements for the deformable PMMA plate specimen with a size of 0.002 mm in the zone near the mould. The total time of the simulation is approximately 60 seconds using a processor of 2.4 GHz and a random-access memory of 8 GHz.

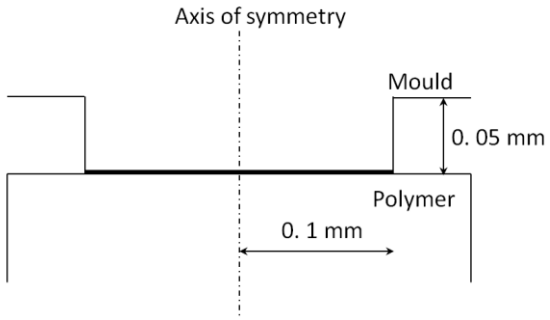

Fig. 6. 2D axisymmetric geometry model used to simulate the micro hot embossing process.

5. Results and discussion

5.1. Numerical simulation of the filling stage of the hot embossing process

The results of the numerical simulation are presented in this section. Different material behaviour laws were applied to the polymer substrate to investigate the influence of the elastic, viscous, and plastic behaviour on the filling efficiency during the micro hot embossing process.

5.1.1. Case of elastic behaviour

First, only the elastic behaviour was considered. The plate specimen was compressed by imposing a displacement on the mould. Figs. 7(a)–(d) show the filling results corresponding to the imposed displacements of 0.05, 0.10, 0.15, and 0.2 mm, respectively. The maximal von Mises stress occurred at the sidewall corner of the mould, independent of the imposed displacement. It reached 1.33 and 3.31 MPa for the lowest and highest values, respectively, of the imposed displacement. The micro-cavity filling efficiency increased with the imposed

displacement. The simulations also revealed a micro-gap corresponding to an unfilled region during the hot embossing for the four imposed displacements.

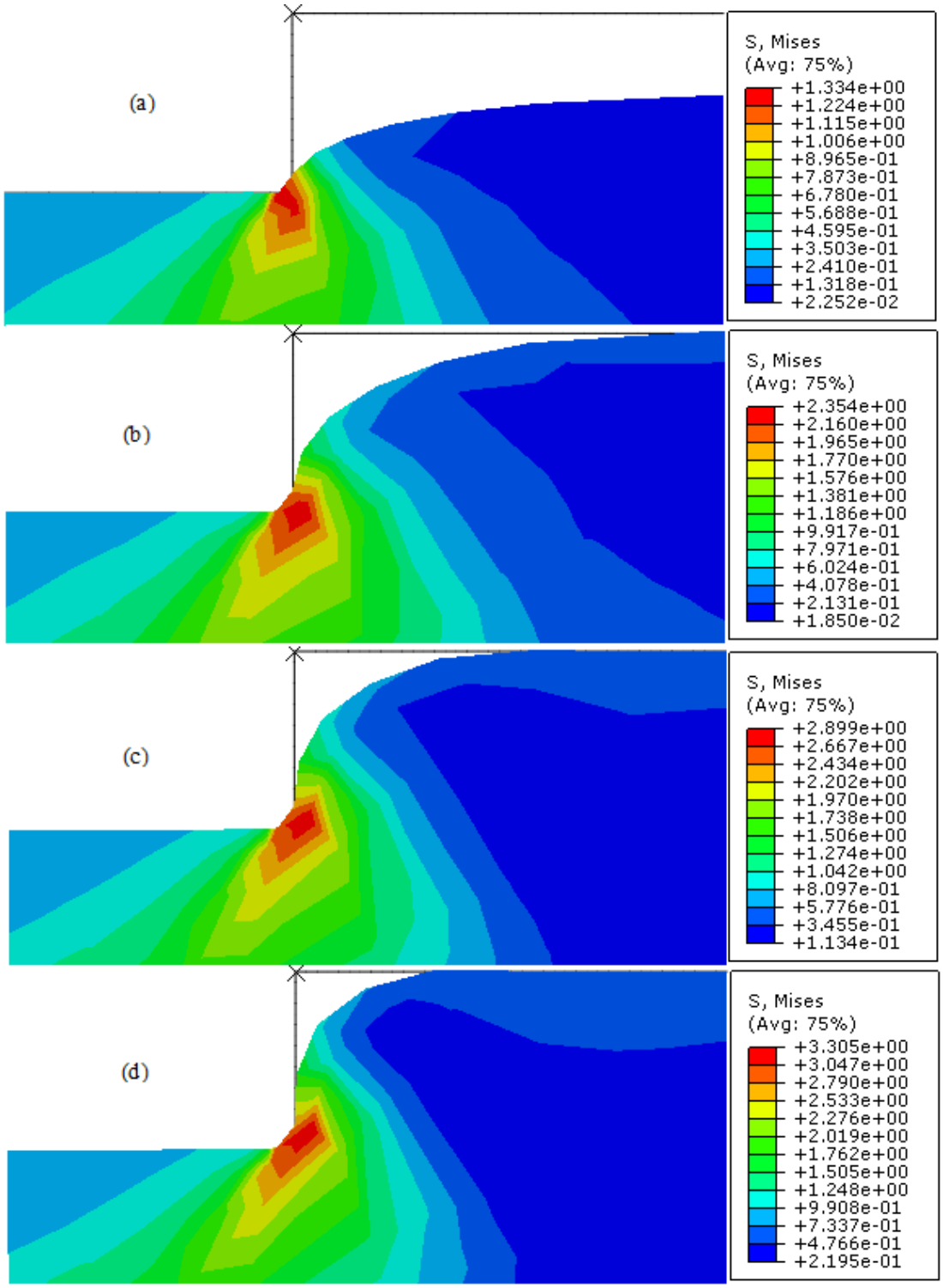

Fig. 7. Distribution of the numerical von Mises stress in the polymer during the hot embossing simulation with the elastic model at $T_g + 20$ °C: (a) d = 0.05 mm, (b) d = 0.1 mm, (c) d = 0.15 mm, and (d) d = 0.2 mm.

5.1.2. Case of elastoplastic behaviour

Next, the plate specimen was compressed by the mould during the hot embossing process with imposed displacements of 0.05, 0.10, 0.15, and 0.2 mm while the elastoplastic constitutive law (Eq. (2)) was considered.

Fig. 8 shows the von Mises stress values of the plate specimen for different imposed displacements during the hot embossing process. The filling efficiency increased with elastoplastic behaviour when compared to just elastic behaviour. The maximal von Mises stress increased from 1.27 MPa to 1.4 MPa as the imposed displacement was increased from 0.05 to 0.2 mm. The zone of the higher stress increased in size with the imposed displacement. The filling efficiency for the micro-cavity increased with the imposed displacement.

Esmaeilpour et al. [29] proposed using the effective strain distribution to quantify the filling efficiency during the modelling and material forming process. For the plate specimen, the effective strain distribution during the hot embossing process can be an effective parameter for comparing the viscoplastic deformation under different loading conditions. Fig. 9 shows the effective plastic strain of the polymer substrate under different imposed displacements. The effective plastic strain of the plate specimen increased with the imposed displacement applied on the mould at the microscale. The maximum effective plastic strain occurred in the corner of the mould at the end of the hot embossing process and increased from 0.26 to 2.86 with the imposed displacement. These results indicate that the plasticity of the amorphous polymer has an important effect on the filling efficiency during the micro hot embossing process.

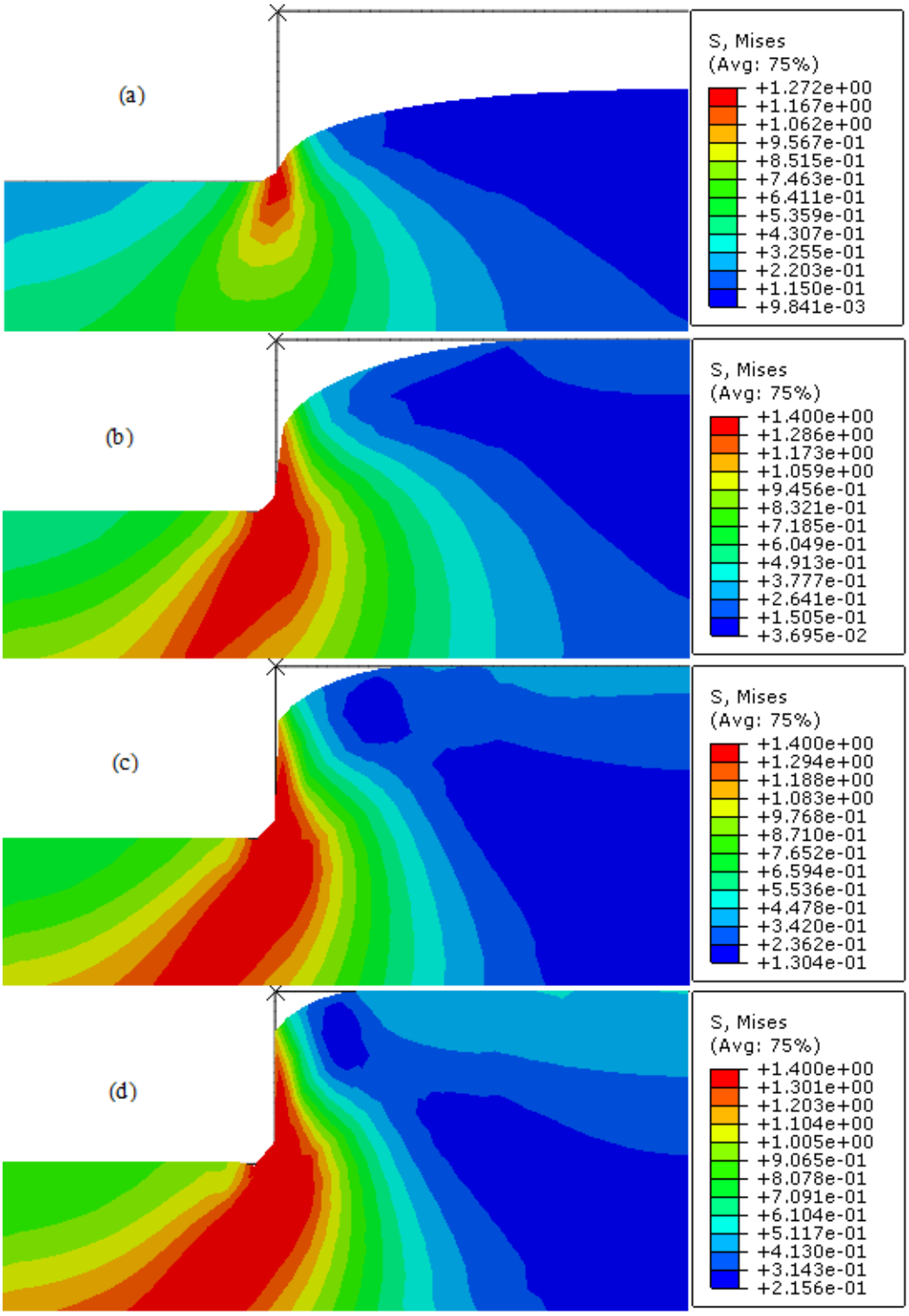

Fig. 8. Von Mises stress distributions during the simulation of the PMMA plate specimen with the elastoplastic model at $T_g + 20$ °C: (a) d = 0.05 mm, (b) d = 0.1 mm, (c) d = 0.15 mm, and (d) d = 0.2 mm.

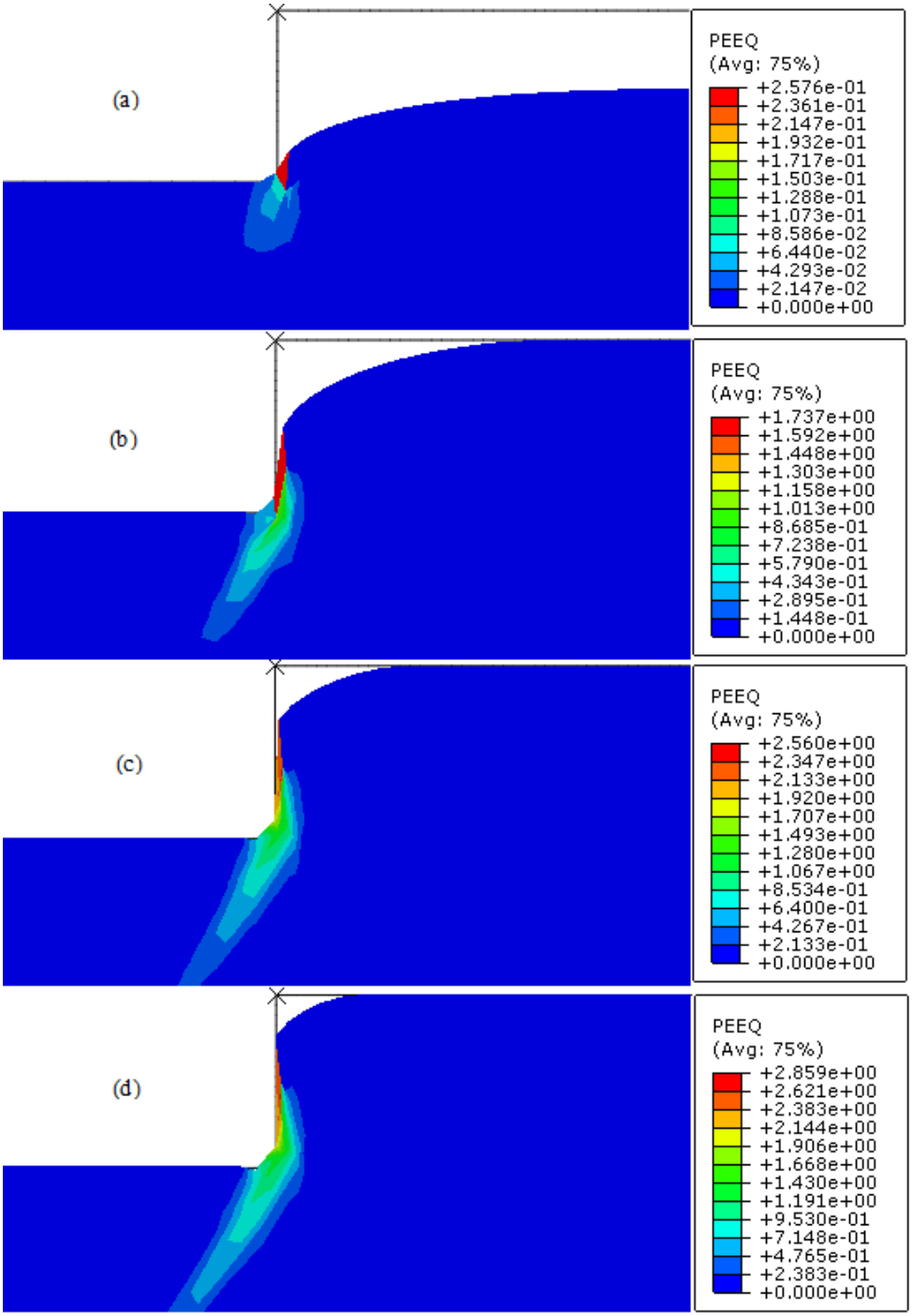

Fig. 9. Distribution of the numerical effective plastic strain in the polymer during the hot embossing simulation with the elastoplastic model at $T_g + 20$ °C: (a) d = 0.05 mm, (b) d = 0.1 mm, (c) d = 0.15 mm, and (d) d = 0.2 mm.

5.1.3. Case of elastic-viscoplastic behaviour

The elastic-viscoplastic constitutive behaviour of the PMMA substrate was considered in the numerical simulation. The parameter f was set to 0.89 (Table 1). Fig. 10 shows the von Mises stress distribution in the plate specimen under different imposed displacements. The maximal von Mises stress increased from 0.356 MPa to 0.504 MPa as the imposed displacement was increased from 0.05 to 0.2 mm, respectively. The cavity filling ratio increased with the imposed displacement. When the imposed displacement was 0.2 mm, the micro-cavity was almost completely filled.

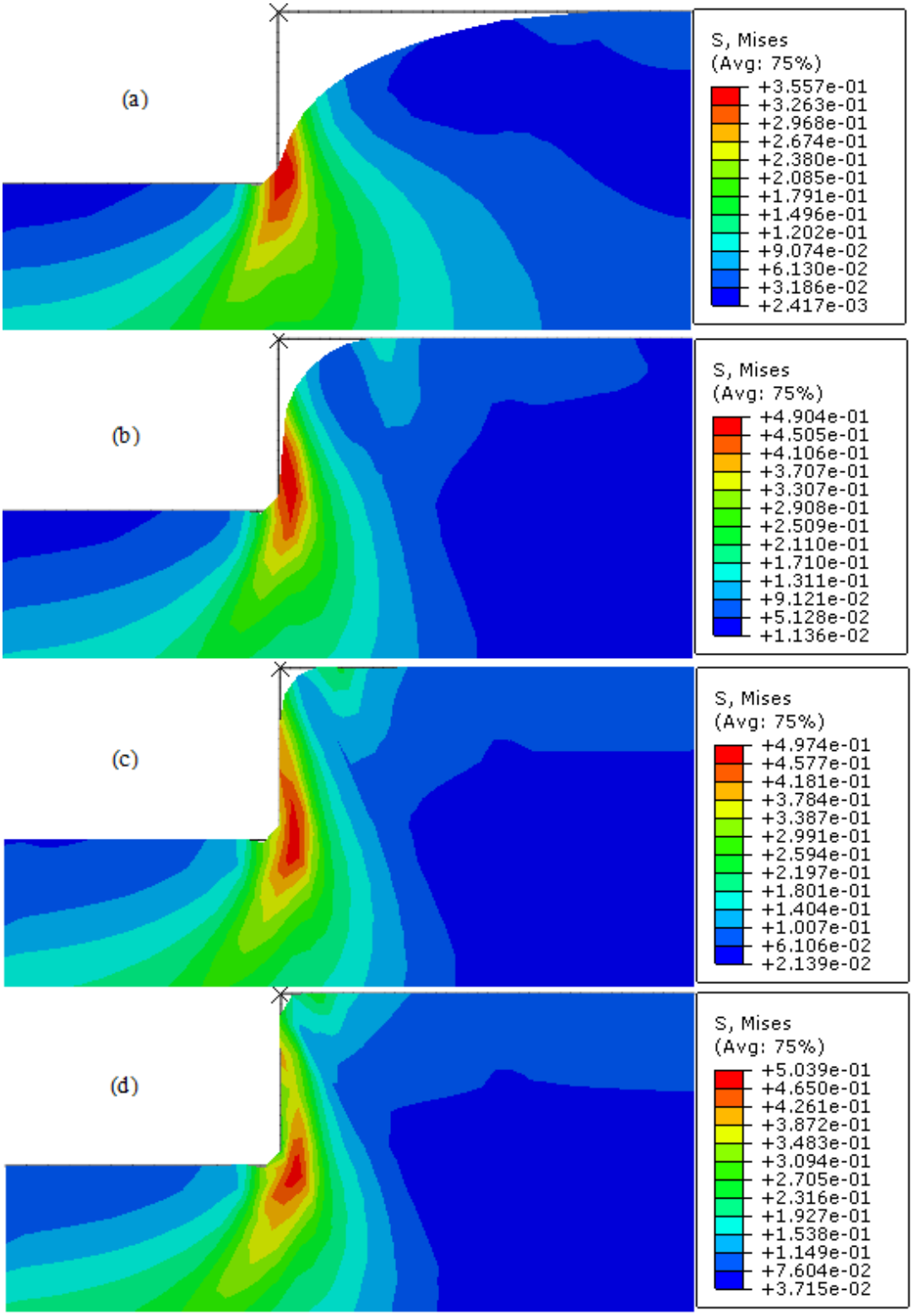

Fig. 10. Von Mises stress results for the PMMA substrate specimen during the whole process with the elastic-viscoplastic model at $T_g + 20$ °C: (a) d = 0.05 mm, (b) d = 0.1 mm, (c) d = 0.15 mm, and (d) d = 0.2 mm.

Fig. 11 shows the effective plastic strain of the polymer substrate under different imposed displacements. No plastic strain was observed with the imposed displacements of 0.05 and 0.1 mm, which was probably because the limit of plasticity was not reached. Little plastic strain was produced with the imposed displacements of 0.15 and 0.2 mm. Plastic strain occurred near the corner of the micro mould die, where the most important deformation of the polymer substrate was located (Figs. 11(c) and (d)). This result is strongly consistent with the polymer's elastoplastic properties in the compression tests. Very little plastic strain was observed in the polymer flow at this temperature range (Table 2).

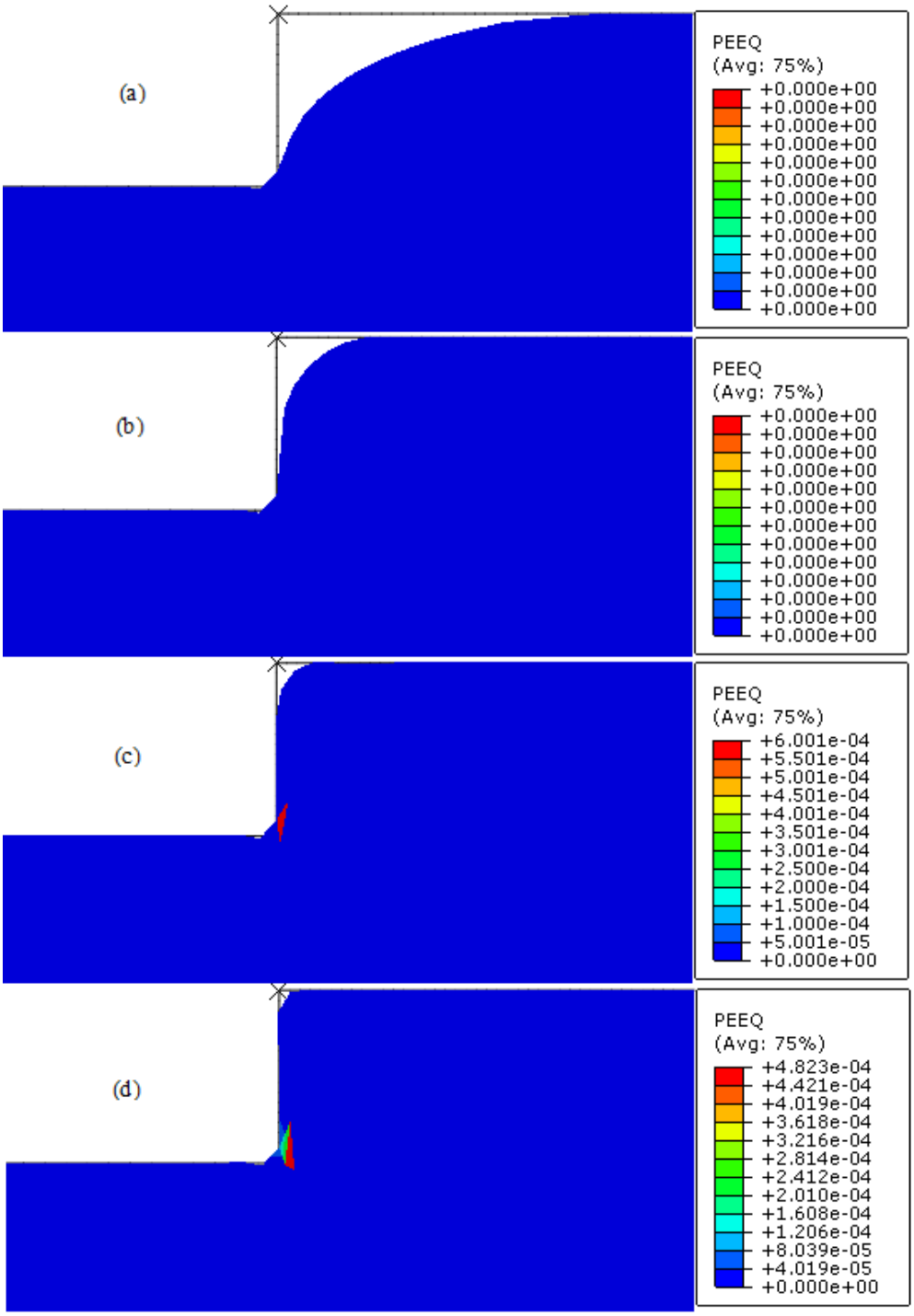

Fig. 11. Distribution of the effective plastic strain in the polymer during the hot embossing simulation with the elastic-viscoplastic model at $T_g + 20$ °C: (a) d = 0.05 mm, (b) d = 0.1 mm, (c) d = 0.15 mm, and (d) d = 0.2 mm.

5.1.4. Summary of different cases

Simulations were performed considering the elastic, elastoplastic, and elastic-viscoplastic behaviours to study the effect of the mechanical constitutive law on the filling efficiency of PMMA during the hot embossing process. Table 3 presents the numerical results for the filling ratio of the cavity under different imposed displacements. The filling ratio increased with the imposed displacement, independent of the material model used. Based on the filling ratios obtained at the same imposed displacement of 0.2 mm, using the elastic-viscoplastic model increased the filling ratio in the numerical simulation. This result demonstrates that the micro-cavity was almost completely filled when the elastic, plastic, and viscous behaviours were all considered during the simulation. The filling ratios with the elastoplastic and elastic-viscoplastic models were used to examine the influence of the viscous behaviour of the polymer substrate on the filling efficiency of the micro-cavity. The unfilled area with the elastoplastic model was ~71 μm^2 for a filling ratio of 97.00% when the imposed displacement was 0.2 mm. The unfilled area with the elastic-viscoplastic model was ~17 μm^2 for a filling ratio of 99.99% under the same imposed displacement. This suggests that the viscosity of polymer material can improve the filling efficiency of the mould cavity during the micro hot embossing process.

Table 3. Cavity filling ratio versus different imposed displacements and constitutive behaviours.

Imposed displacement (mm)	Filling ratio		
	Elastic	Elastoplastic	Elastic-viscoplastic
0.05	43.00%	46.00%	98.40%
0.10	88.00%	91.25%	98.90%
0.15	91.50%	95.00%	99.16%
0.20	95.34%	97.00%	99.99%

5.2. Sensitivity of the two-layer viscoplastic model to the parameter f

f is the most important parameter for the two-layer viscoplastic model (Eq. (1)). It signifies the ratio of the elastic modulus in the viscoelastic branch to the total elastic modulus and varies from 0 to 1. When f is relatively large, this means that the material exhibits more elastic behaviour in the viscoelastic branch than in the elastoplastic branch. This would indicate that the elastic deformation in the viscoelastic branch dominates the total deformation of the material.

Based on the results obtained in previous section, the micro cavities were completely filled when using the elastic-viscoplastic model, in which f was set to 0.89 according to the characterisation by the compression tests. However, four values of f = 0.2, 0.4, 0.6 and 0.8 were arbitrary considered to analyse the influence of this parameter on the filling efficiency of the micro hot embossing process. All the other material parameters were kept constant. Figs. 12(a)–(d) show the corresponding distributions of the von Mises stress for the polymer substrate in the numerical simulation. The maximum von Mises stress decreased from 1.549 MPa to 0.88 MPa with increasing f. This may indicate that the polymer substrate comes

under less stress when more elasticity is located in the viscoelastic branch. The mould cavity was filled more by the polymer when f was increased, which indicates that the elasticity in the viscoelastic branch improves the filling efficiency of the amorphous polymer during the micro hot embossing process.

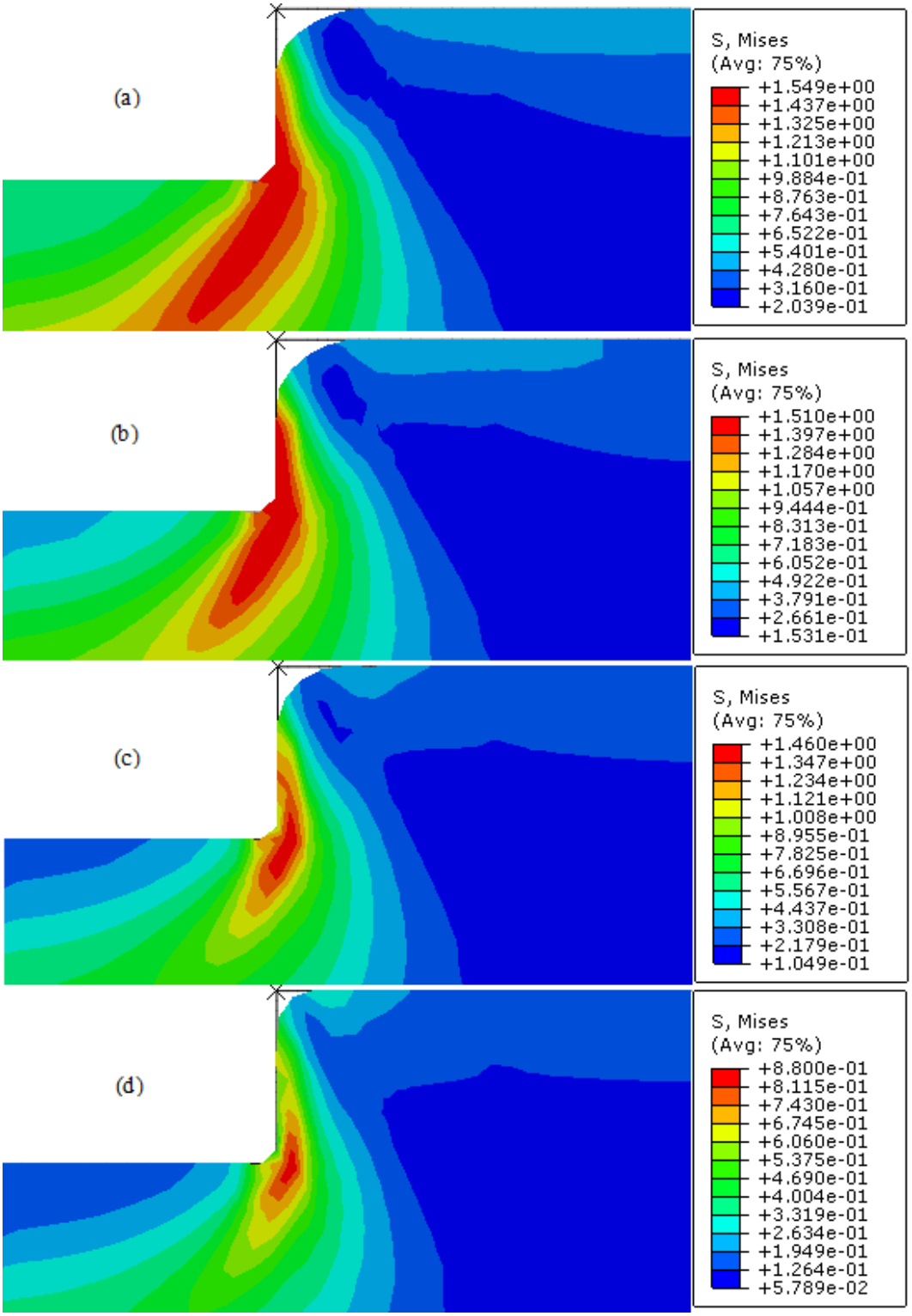

Fig. 12. Von Mises stress results for the PMMA substrate specimen with elastic-viscoplastic behaviour at $T_g + 20$ °C and (a) $f = 0.2$, (b) $f = 0.4$, (c) $f = 0.6$, and (d) $f = 0.8$.

5.3. Experimental validation of the numerical results

The proposed material model for the micro hot embossing process needed to be validated experimentally. Cheng et al. [12] developed a complete injection-compression microfluidic mould die (Fig. 13(a)) to fabricate microfluidic devices, which comprises heating, cooling, ejection, and vacuum systems. The microfluidic mould die was made of steel and the micro cavities in the mould were elaborated by laser ablation with laser micro manufacturing equipment, corresponding to a lens of 160 mm focal length with a spot diameter of 25 µm. The specific mould was installed in injection equipment (Billion® SELECT) with a maximum clamping force of 500 kN. Fig. 13(a) shows a detailed image of the microfluidic features in the specific mould and the reservoir zone marked with a red circle corresponding to the numerical geometry model for the simulation. PMMA microfluidic devices with heights of 0.05, 0.1, and 0.2 mm were successfully replicated by hot embossing. The devices were characterised by optical 3D measurements to analyse the filling efficiency of the micro die cavity. Fig. 13(b) shows the reservoir zone of the replicated polymer substrate obtained by the microfluidic mould (height of 0.05 mm). The 3D image was cut along a plane passing through the centre of the reservoir (marked in red in Fig. 13(b)) and a detailed cross-sectional profile was shown to measure the height of the filling materials. This zone was considered because it exhibited the same geometry specific to the numerical model used for the simulations. Fig. 13(b) shows that the micro die cavity in the reservoir zone was completely filled, which correlates with the numerical simulation results for the micro hot embossing process. This agreement with the experimental results verified that the proposed elastic-viscoplastic model effectively describes the thermoplastic constitutive behaviour during the micro hot embossing process.

Cheng et al. [12] fabricated PMMA microfluidic devices at different embossing temperatures slightly above T_g. The micro die cavity was filled more when the embossing temperature was

increased, which caused the polymer flow to exhibit more viscous behaviour. This correlates with the numerical simulation results obtained with the elastoplastic and elastic viscoplastic models. The filling efficiency of the micro hot embossing process can be improved if the polymer substrate is more viscous.

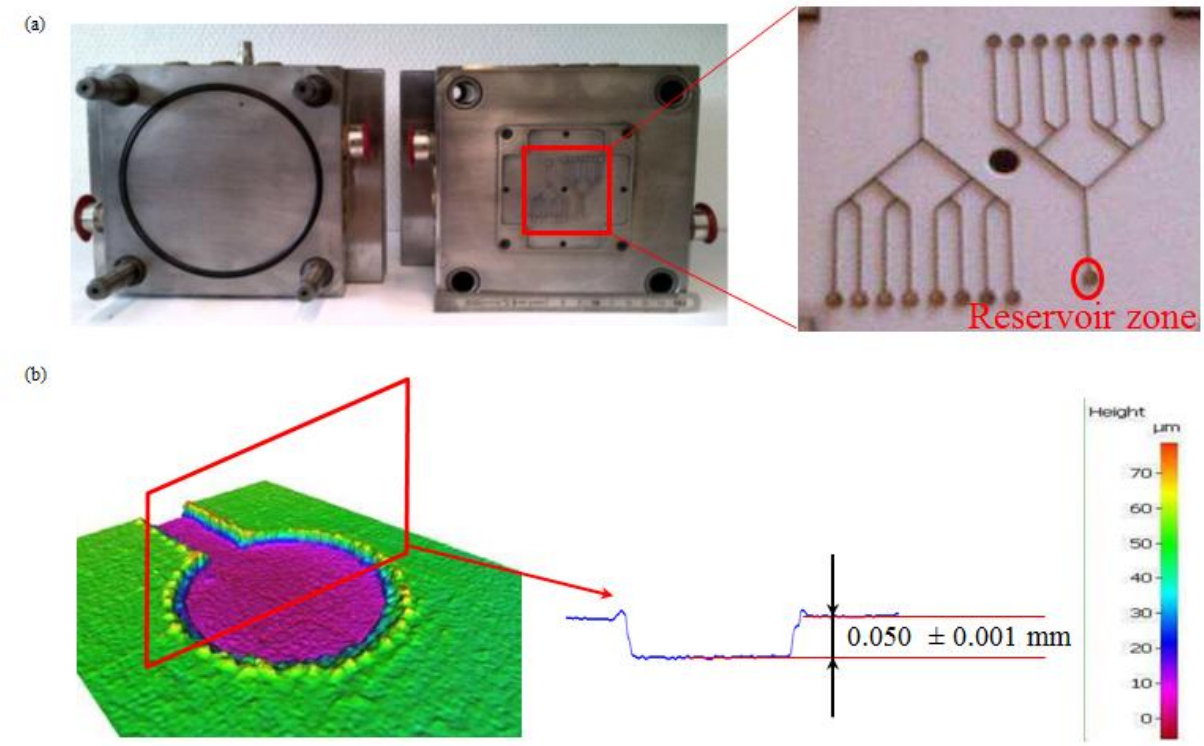

Fig. 13. (a) Microfluidic mould die features with associated reservoir zone corresponding to the numerical geometry model (b) The reservoir zone of the replicated PMMA microfluidic mould with a detailed cross-sectional profile.

6. Conclusion

The aim of this study was to investigate the influence of the elastic, elastoplastic, and elastic viscoplastic behaviours of polymers, especially PMMA, on the filling efficiency of the micro hot embossing process. Three benchmark cases were considered to investigate the effect of polymer properties on the filling ratio of the micro-cavity and validate the model for the micro

hot embossing process: elastic behaviour, elastoplastic behaviour, and elastic-viscoplastic behaviour, at a temperature slightly above T_g ($T_g + 20$ °C). The simulation results showed that the filling efficiency increased with the imposed displacement. The cavity was completely filled with the elastic-viscoplastic model, which indicates the importance of viscous behaviour for the filling efficiency of the micro hot embossing process. The sensitivity of the proposed elastic-viscoplastic model was investigated by conducting numerical simulations for several values of the parameter f corresponding to the ratio of the elastic modulus of the viscoelastic branch to the total modulus. The results showed that the micro-cavity was filled more when f was close to 0.8, which indicates that increasing the elasticity in the viscoelastic branch can improve the filling efficiency of the polymer flow during the micro hot embossing process. A high filling ratio in the reservoir area was observed in the experiments, which verified the effectiveness of the selected elastic-viscoplastic model in the numerical simulation of the filling stage of the micro hot embossing process. The numerical analyses showed excellent agreement with the experimental observations for the fabrication of microfluidic devices.

The proposed material model provides several advantages compared to currently available methods, such as identification of fewer material parameters, compatibility with simulation software, and high parameter sensitivity. Future work can involve extending this model to the simulation of the filling stage with PMMA and other kinds of polymers under other temperature conditions.

Acknowledgements

The authors wish to acknowledge the financial support received from LaMé and INSA Centre Val de Loire to achieve this work. This research work was also supported by the EIPHI Graduate School (contract ANR-17-EURE-0002) and the French “Investissements d’Avenir” program, project ISITE-BFC (contract ANR-15-IDEX-0003).

References

[1] Trotta G, Volpe A, Ancona A, Fassi I. Flexible micro manufacturing platform for the fabrication of PMMA microfluidic devices. J. Manuf. Process. 2018;35:107–117. https://doi: 10.1016/j.jmapro.2018.07.030

[2] Sucularli F, Sahir Arikan MA, Yildirim E. Investigation of process-affected zone in ultrasonic embossing of microchannels on thermoplastic substrates. J. Manuf. Process. 2020;50:394–402. https://doi.org/10.1016/j.jmapro.2019.12.055

[3] Lin CR, Chen RH, Hung C. Preventing non-uniform shrinkage in open-die hot embossing of PMMA microstructures. J. Mater. Process. Technol. 2003;140:173–178. https://doi.org/10.1016/S0924-0136(03)00709-X

[4] Chien CH, Yu HM. The novel fabrication of multi-metal layers embedded in PMMA polymer material. J. Mater. Process. Technol. 2007;187-188:314–317. https://doi.org/10.1016/j.jmatprotec.2006.11.197

[5] Cheng G, Sahli M, Gelin JC, Barrière T. Process parameter effects on dimensional accuracy of a hot embossing process for polymer-based micro-fluidic device manufacturing. Int. J. Adv. Manuf. Technol. 2014;75:225–235. https://doi.org/10.1007/s00170-014-6135-6

[6] Huang G, Lu H. Measurements of two independent viscoelastic functions by nanoindentation. Exp. Mech. 2007;47:87–98. https://doi.org/10.1007/s11340-006-8277-4

[7] Cheng E, Yin Z, Zou H, Chen L. Surface modification-assisted bonding of 2D polymer-based nanofluidic devices. Microfluid. Nanofluid. 2015;18:527–535. https://doi.org/s10404-014-1451-6

[8] Wang J, Yi P, Deng Y, Peng L, Lai X, Ni J. Recovery behavior of thermoplastic polymers in micro hot embossing process. J. Mater. Process. Technol. 2017;243:205–216. https://dx.doi.org/10.1016/j.jmatprotec.2016.12.024

[9] He J, Wu M, Zhang R, Liu J, Deng Y, Guo Z. A one-step hot-embossing process for fabricating a channel with superhydrophobic inner walls. J. Manuf. Process. 2018;36:351–359. https://doi.org/10.1016/j.jmapro.2018.10.036

[10] Hu M, Xie J, Li W, Lu K. Study on non-isothermal hot-embossing of polymer micro-prism array with efficiency and accuracy. J. Mater. Process. Technol. 2019;266:675–686. https://doi.org/10.1016/j.jmatprotec.2018.11.041

[11] Delorenzi HG, Nied HF. Blow molding and thermoforming of plastics: Finite element modeling. Comput. Struct. 1987;26:197-206. https://doi.org/10.1016/0045-7949(87)90250-1

[12] Cheng G, Sahli M, Gelin JC, Barrière T. Physical modelling, numerical simulation and experimental investigation of microfluidic devices with amorphous thermoplastic polymers using a hot embossing process. J. Mater. Process. Technol. 2016;229:36–53. https://doi.org/10.1016/j.jmatprotec.2015.08.027
[13] Wang J, Xu Y, Zhang W, Moumni Z. A damage-based elastic-viscoplastic constitutive model for amorphous glassy polycarbonate polymers. Mater. Design 2016;97:519–531. https://doi.org/10.1016/j.matdes.2016.02.118
[14] Covezzi F, Miranda SD, Marfia S, Sacco E. Homogenization of elastic-viscoplastic composites by the mixed TFA. Comput. Methods Appl. Mech. Engrg. 2017;318:701–723. https://doi.org/10.1016/j.cma.2017.02.009
[15] Gudimetla MR, Doghri I. A finite strain thermodynamically-based constitutive framework coupling viscoelasticity and viscoplasticity with application to glassy polymers. Int. J. Plast. 2017;98:197–216. https://doi.org/10.1016/j.ijplas.2017.08.001
[16] Holopainen S, Barrière T. Modeling of mechanical behavior of amorphous solids undergoing fatigue loadings, with application to polymers. Comput. Struct. 2018;199:57–73. https://doi.org/10.1016/j.compstruc.2018.01.010
[17] Sorini C, Chattopadhyay A, Goldberg RK. An improved plastically dilatant unified viscoplastic constitutive formulation for multiscale analysis of polymer matrix composites under high strain rate loading. Compos. Part B-Eng. 2020;184:107669. https://doi.org/10.1016/j.compositesb.2019.107669
[18] Farias JC, Stainier L, Fancello EA. A variational framework for the modeling of glassy polymers under finite strains. Continuum Mech. Thermodyn. 2019 https://doi.org/10.1007/s00161-019-00809-8
[19] Wang J, Peng LF, Deng YJ, Lai XM, Fu MW, Ni J. A finite strain thermodynamically-based constitutive modeling and analysis of viscoelastic-viscoplastic deformation behavior of glassy polymers. Int. J. Plasticity 2019;122:135–163. https://doi.org/10.1016/j.ijplas.2019.06.013
[20] Mahjoubi H, Zaïri F, Tourki Z. A micro-macro constitutive model for strain-induced molecular ordering in biopolymers: Application to polylactide over a wide range of temperatures. Int. J. Plasticity 2019;123:38–55. https://doi.org/10.1016/j.ijplas.2019.07.001
[21] Niyonzima I, Jiao Y, Fish J. Modeling and simulation of nonlinear electro-thermo-mechanical continua with application to shape memory polymeric medical devices. Comput. Methods Appl. Mech. Engrg. 2019;350:511–534. https://doi.org/10.1016/j.cma.2019.03.003

[22] Cheng G, Barrière T. Effect of viscoplasticity on microfluidic cavity filling efficiency of a thermoplastic polymer in hot-embossing process. Int. J. Adv. Manuf. Technol. 2019;103:549–565. https://doi.org/10.1007/s00170-019-03447-1
[23] Charkaluk E, Bignonnet A, Constantinescu A, Dang Van K. Fatigue design of structures under thermomechanical loadings. Fatigue Fract. Eng. Mater. Struct. 2002;25:1199–1206. https://doi.org/10.1046/j.1460-2695.2002.00612.x
[24] Leen SB, Deshpande A, Hyde TH. Experimental and numerical characterization of the cyclic thermomechanical behavior of a high temperature forming tool alloy. J. Manuf. Sci. Eng. 2010;132:051013. https://doi.org/10.1115/1.4002534
[25] Berezvai S, Kossa A. Characterization of a thermoplastic foam material with the two-layer viscoplastic model. Mater. Today Proc. 2017;4:5749–5754. https://doi.org/10.1016/j.matpr.2017.06.040
[26] Abdel-Wahab AA, Ataya S, Silberschmidt VV. Temperature-dependent mechanical behaviour of PMMA: Experimental analysis and modelling. Polym. Test. 2017;58:86–95. https://doi.org/10.1016/j.polymertesting.2016.12.016
[27] Alipour Skandani A, Al-Haik M. Viscoplastic characterization and modeling of hybrid carbon fiber/carbon nanotubes reinforced composites. Compos. Part B-Eng. 2016;99:63–74. https://doi.org/10.1016/j.compositesb.2016.06.029
[28] Nguyen-Thanh VM, Zhuang X, Nguyen-Xuan H, Rabczuk T, Wriggers P. A virtual element method for 2D linear elastic fracture analysis. Comput. Methods Appl. Mech. Engrg. 2018;340:366–395. https://doi.org/10.1016/j.cma.2018.05.021
[29] Esmaeilpour R, Kim H, Park T, Pourboghrat F, Xu Z, Mohammed B, Abu-Farha F. Calibration of Barlat Yld2004-18P yield function using CPFEM and 3D RVE for the simulation of single point incremental forming (SPIF) of 7075-O aluminum sheet. Int. J. Mech. Sci. 2018;145:24–41. https://doi.org/10.1016/j.ijmecsci.2018.05.015

Fig. captions

Fig. 1. One-dimensional idealisation of the two-layer viscoplastic model.

Fig. 2. Experimental setup for mechanical tests (Bose® Electro Force® instrument): (a) overview of the equipment and (b) magnified view of the specimen.

Fig. 3. Schematic of the uniaxial mechanical test with a specimen.

Fig. 4. Stress–strain curve for the compression behaviour of PMMA at $T_g + 20$ °C.

Fig. 5. Flowchart for integration of the two-layer viscoplastic model in the numerical simulation.

Fig. 6. 2D axisymmetric geometry model used to simulate the micro hot embossing process.

Fig. 7. Distribution of the numerical von Mises stress in the polymer during the hot embossing simulation with the elastic model at $T_g + 20$ °C: (a) d = 0.05 mm, (b) d = 0.1 mm, (c) d = 0.15 mm, and (d) d = 0.2 mm.

Fig. 8. Von Mises stress distributions during the simulation of the PMMA plate specimen with the elastoplastic model at $T_g + 20$ °C: (a) d = 0.05 mm, (b) d = 0.1 mm, (c) d = 0.15 mm, and (d) d = 0.2 mm.

Fig. 9. Distribution of the numerical effective plastic strain in the polymer during the hot embossing simulation with the elastoplastic model at $T_g + 20$ °C: (a) d = 0.05 mm, (b) d = 0.1 mm, (c) d = 0.15 mm, and (d) d = 0.2 mm.

Fig. 10. Von Mises stress results for the PMMA substrate specimen during the whole process with the elastic-viscoplastic model at $T_g + 20$ °C: (a) d = 0.05 mm, (b) d = 0.1 mm, (c) d = 0.15 mm, and (d) d = 0.2 mm.

Fig. 11. Distribution of the effective plastic strain in the polymer during the hot embossing simulation with the elastic-viscoplastic model at $T_g + 20$ °C: (a) d = 0.05 mm, (b) d = 0.1 mm, (c) d = 0.15 mm, and (d) d = 0.2 mm.

Fig. 12. Von Mises stress results for the PMMA substrate specimen with elastic-viscoplastic behaviour at $T_g + 20$ °C and (a) $f = 0.2$, (b) $f = 0.4$, (c) $f = 0.6$, and (d) $f = 0.8$.

Fig. 13. (a) Microfluidic mould die features with associated reservoir zone corresponding to the numerical geometry model (b) The reservoir zone of the replicated PMMA microfluidic mould with a detailed cross-sectional profile.

Table captions

Table 1. Two-layer viscoplastic model parameters of PMMA at $T_g + 20$ °C

Table 2. Plastic strain of PMMA at $T_g + 20$ °C.

Table 3. Cavity filling ratio versus different imposed displacements and constitutive behaviours.

Figure

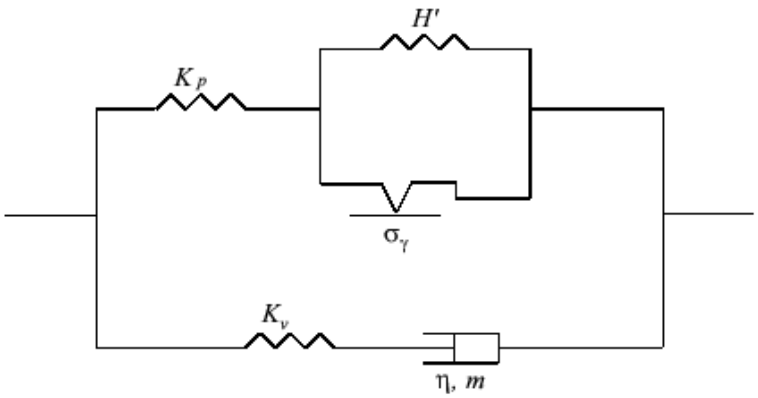

Fig. 1. One-dimensional idealisation of the two-layer viscoplastic model.

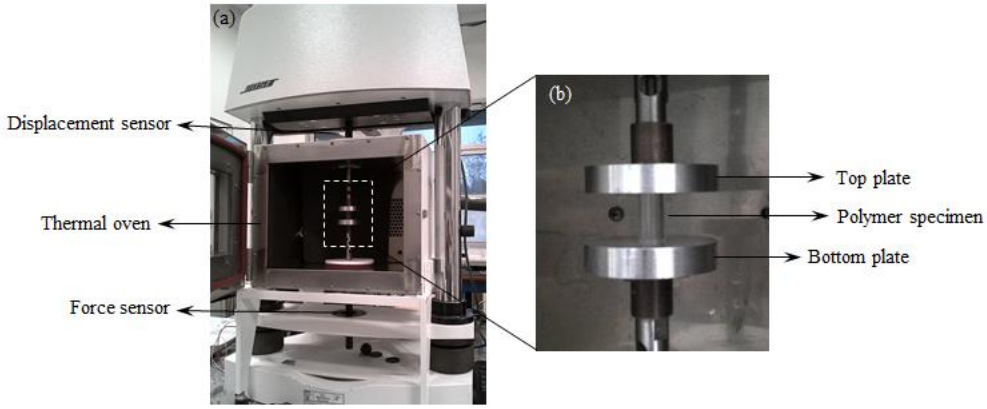

Fig. 2. Experimental setup for mechanical tests (Bose® Electro Force® instrument): (a) overview of the equipment and (b) magnified view of the specimen.

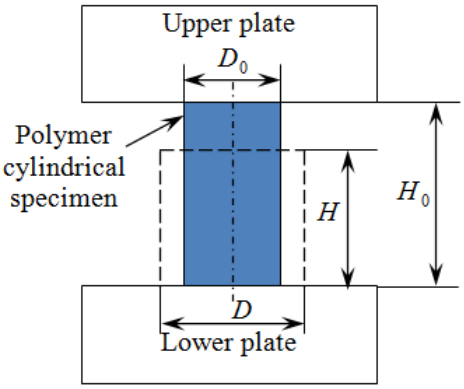

Fig. 3. Schematic of the uniaxial mechanical test with a specimen.

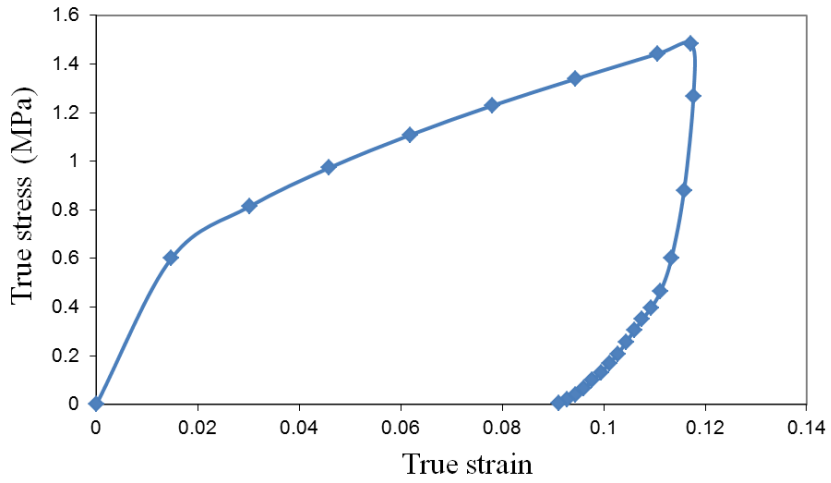

Fig. 4. Stress–strain curve for the compression behaviour of PMMA at $T_g + 20$ °C.

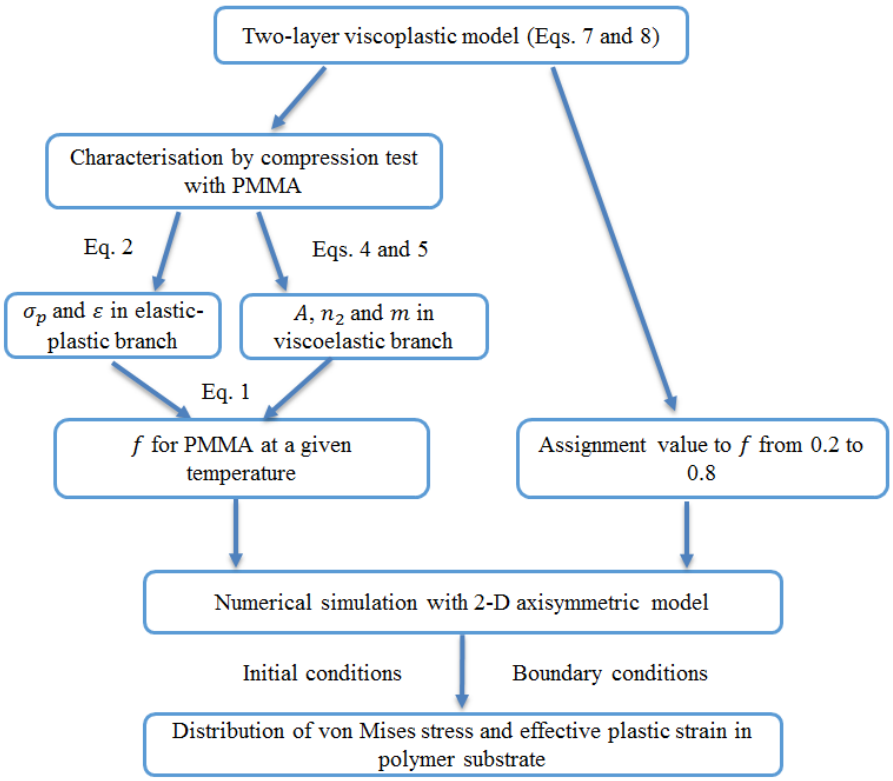

Fig. 5. Flowchart for integration of the two-layer viscoplastic model in the numerical simulation.

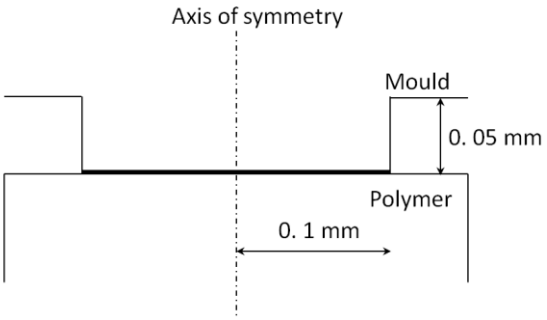

Fig. 6. 2D axisymmetric geometry model used to simulate the micro hot embossing process.

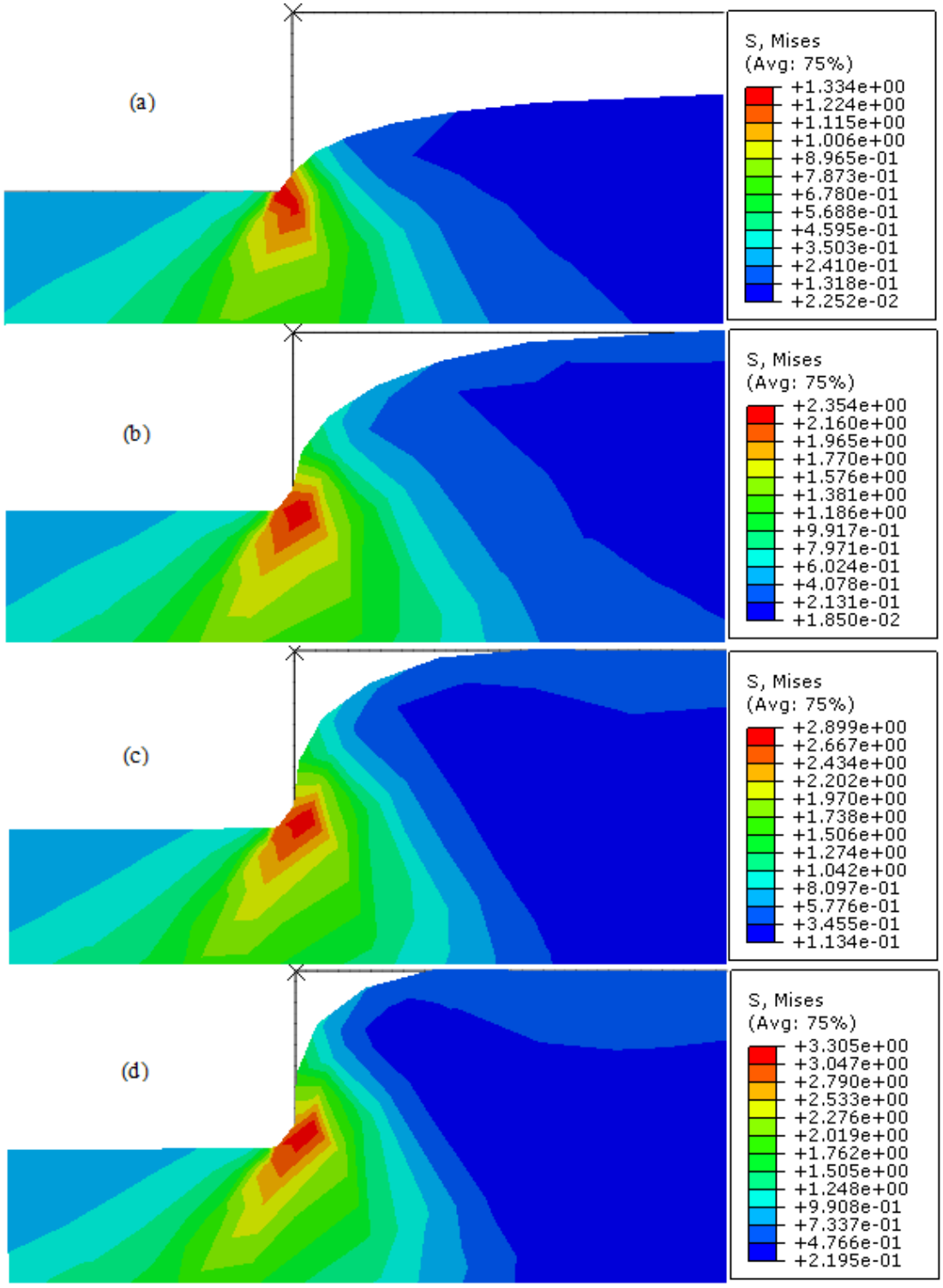

Fig. 7. Distribution of the numerical von Mises stress in the polymer during the hot embossing simulation with the elastic model at $T_g + 20$ °C: (a) d = 0.05 mm, (b) d = 0.1 mm, (c) d = 0.15 mm, and (d) d = 0.2 mm.

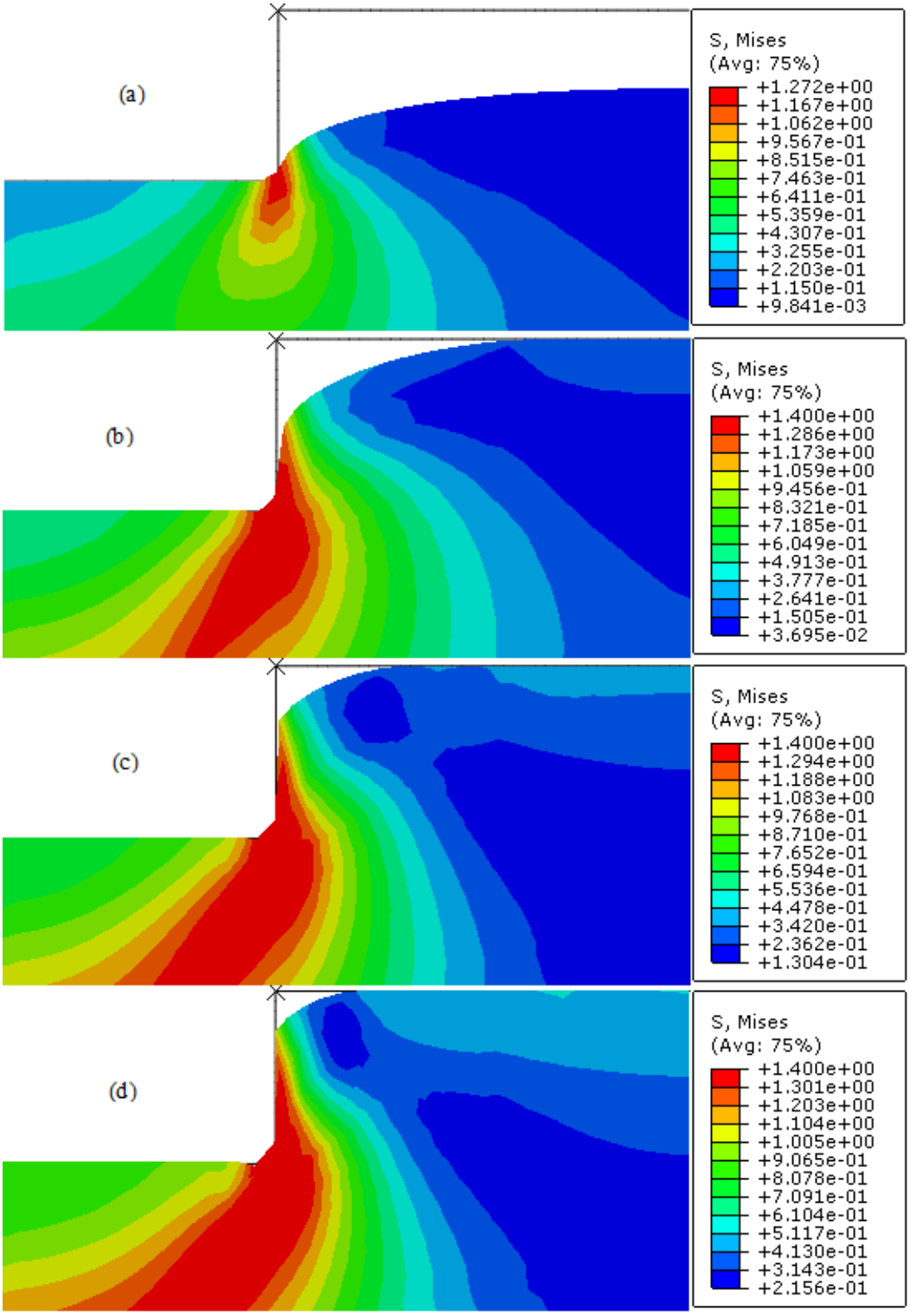

Fig. 8. Von Mises stress distributions during the simulation of the PMMA plate specimen with the elastoplastic model at $T_g + 20$ °C: (a) d = 0.05 mm, (b) d = 0.1 mm, (c) d = 0.15 mm, and (d) d = 0.2 mm.

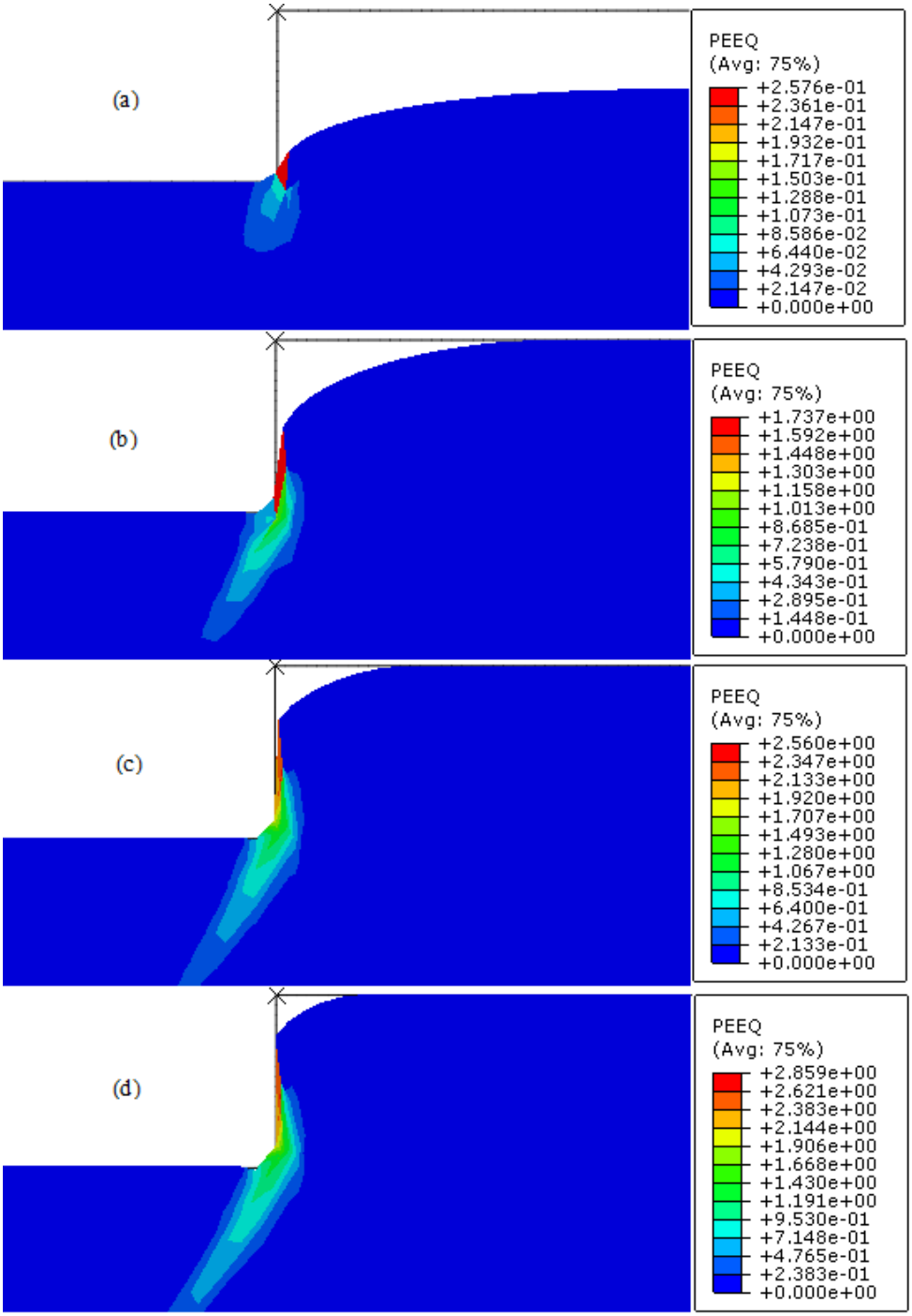

Fig. 9. Distribution of the numerical effective plastic strain in the polymer during the hot embossing simulation with the elastoplastic model at $T_g + 20$ °C: (a) d = 0.05 mm, (b) d = 0.1 mm, (c) d = 0.15 mm, and (d) d = 0.2 mm.

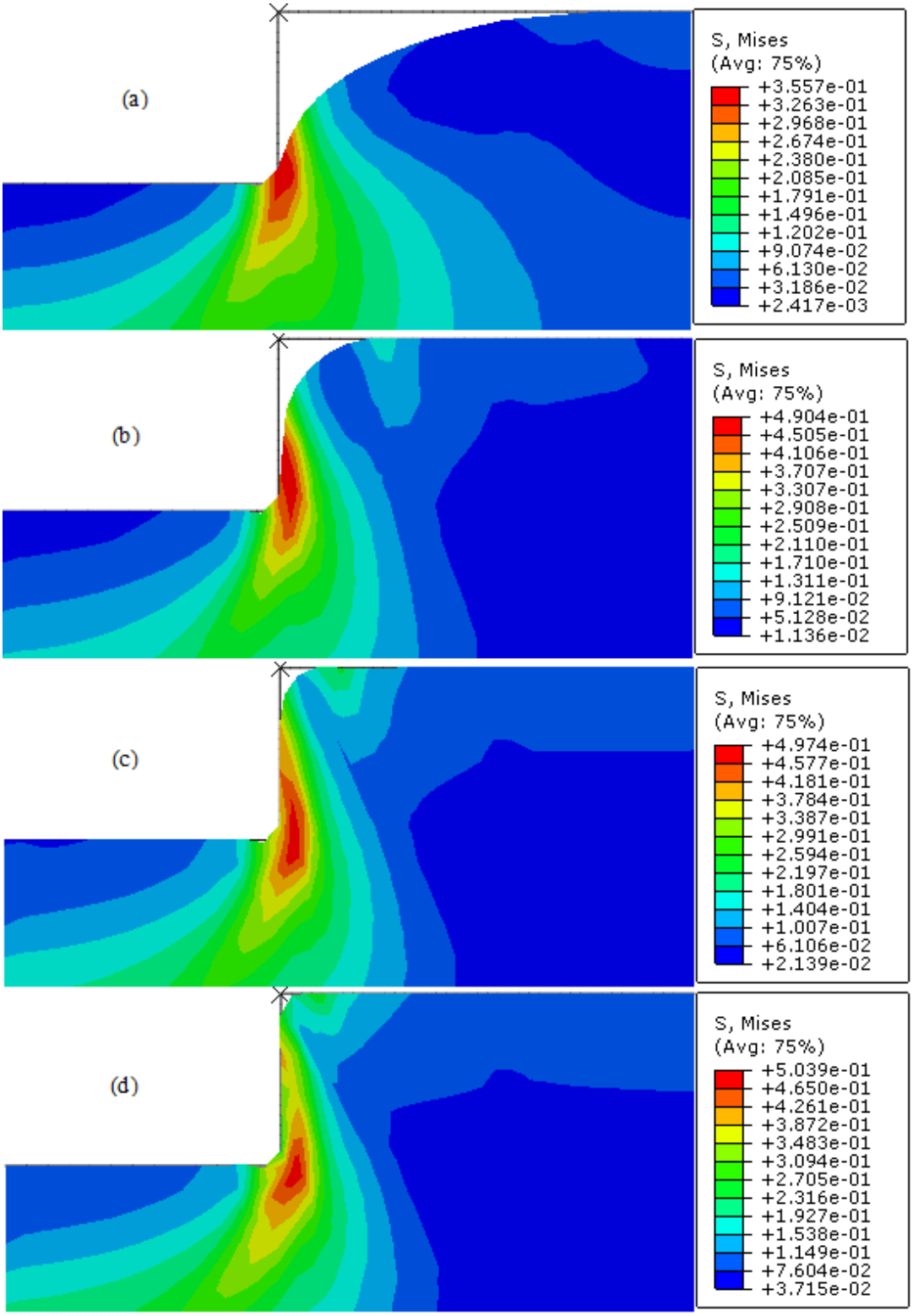

Fig. 10. Von Mises stress results for the PMMA substrate specimen during the whole process with the elastic-viscoplastic model at $T_g + 20$ °C: (a) d = 0.05 mm, (b) d = 0.1 mm, (c) d = 0.15 mm, and (d) d = 0.2 mm.

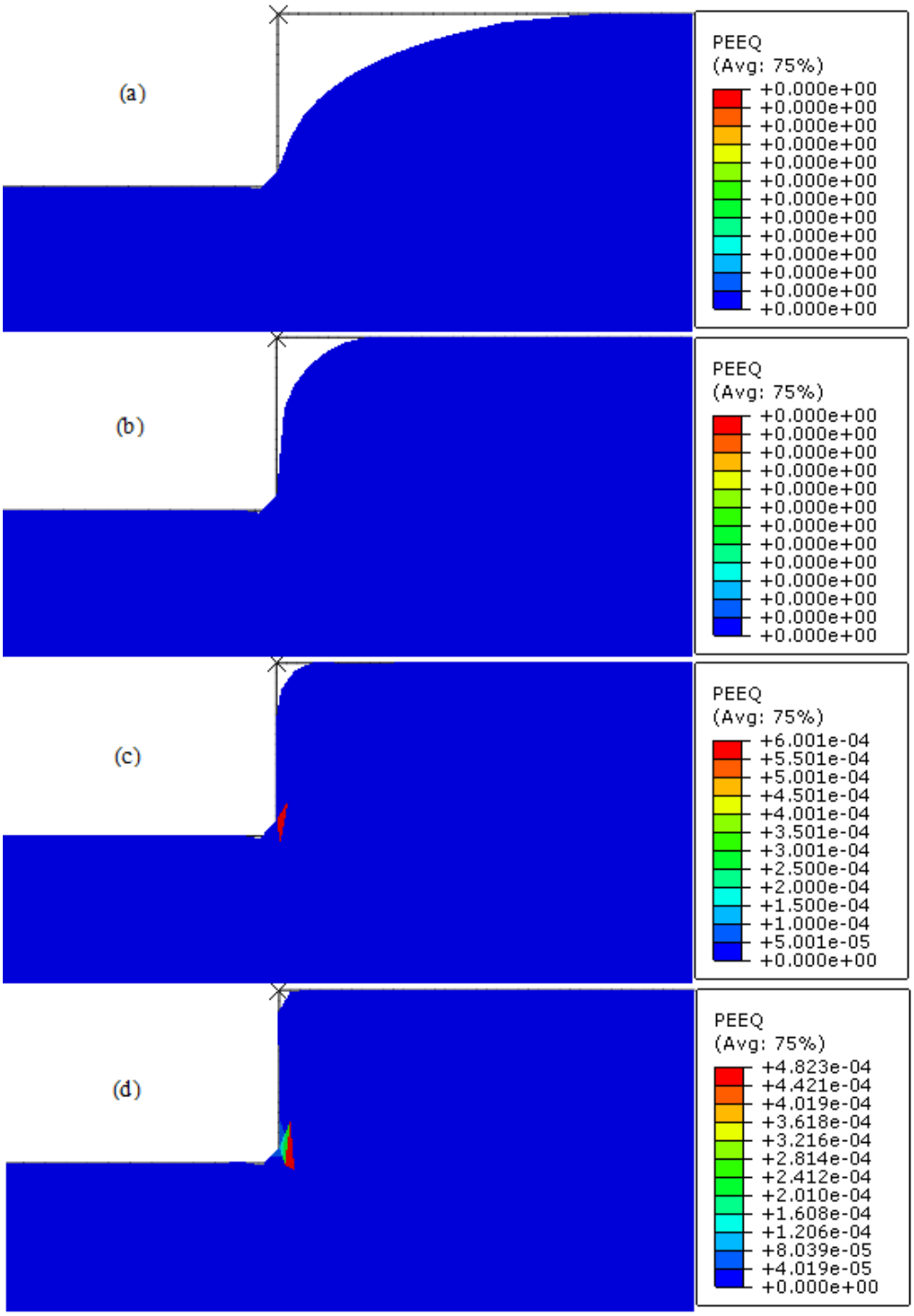

Fig. 11. Distribution of the effective plastic strain in the polymer during the hot embossing simulation with the elastic-viscoplastic model at $T_g + 20$ °C: (a) d = 0.05 mm, (b) d = 0.1 mm, (c) d = 0.15 mm, and (d) d = 0.2 mm.

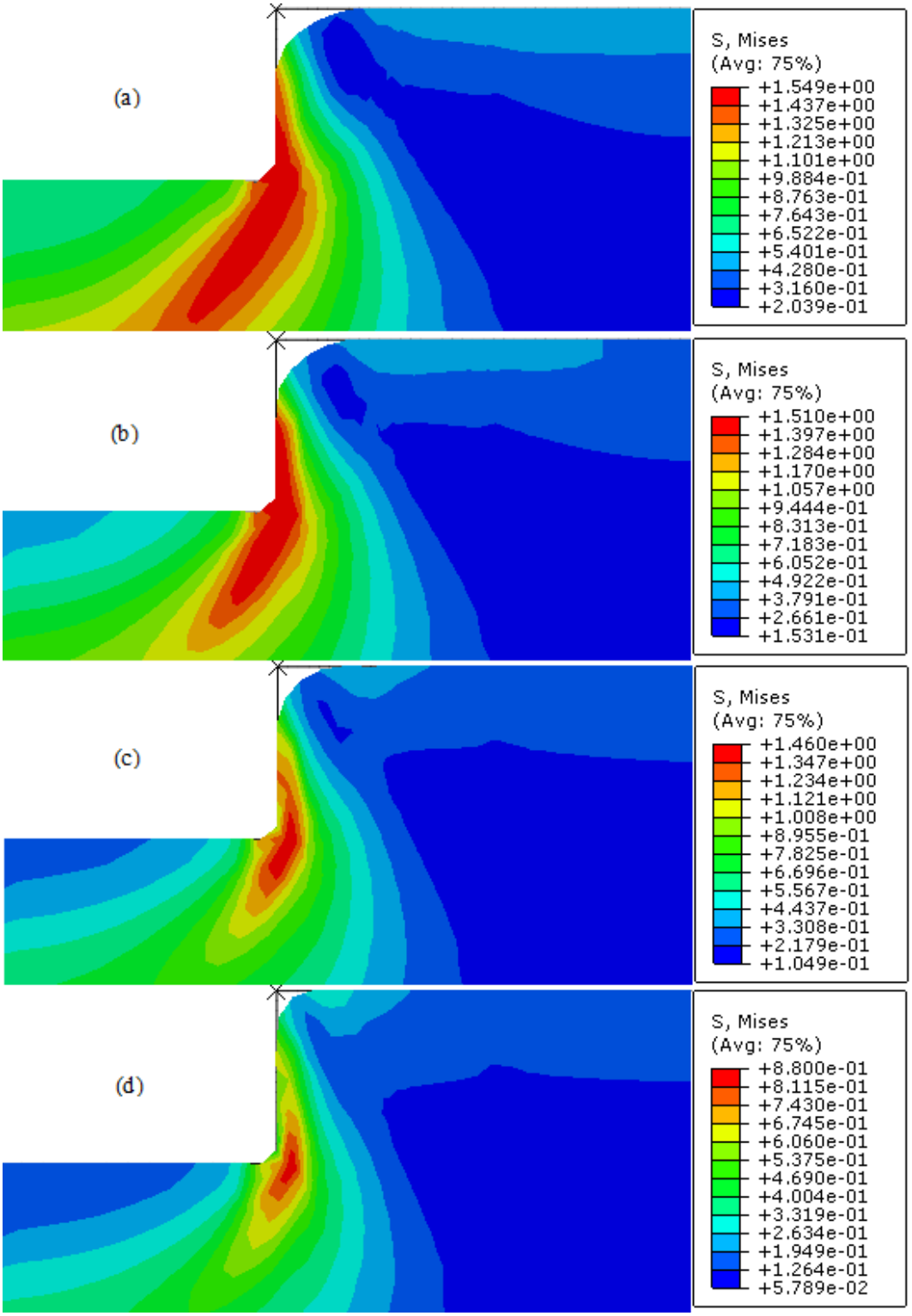

Fig. 12. Von Mises stress results for the PMMA substrate specimen with elastic-viscoplastic behaviour at $T_g + 20$ °C and (a) $f = 0.2$, (b) $f = 0.4$, (c) $f = 0.6$, and (d) $f = 0.8$.

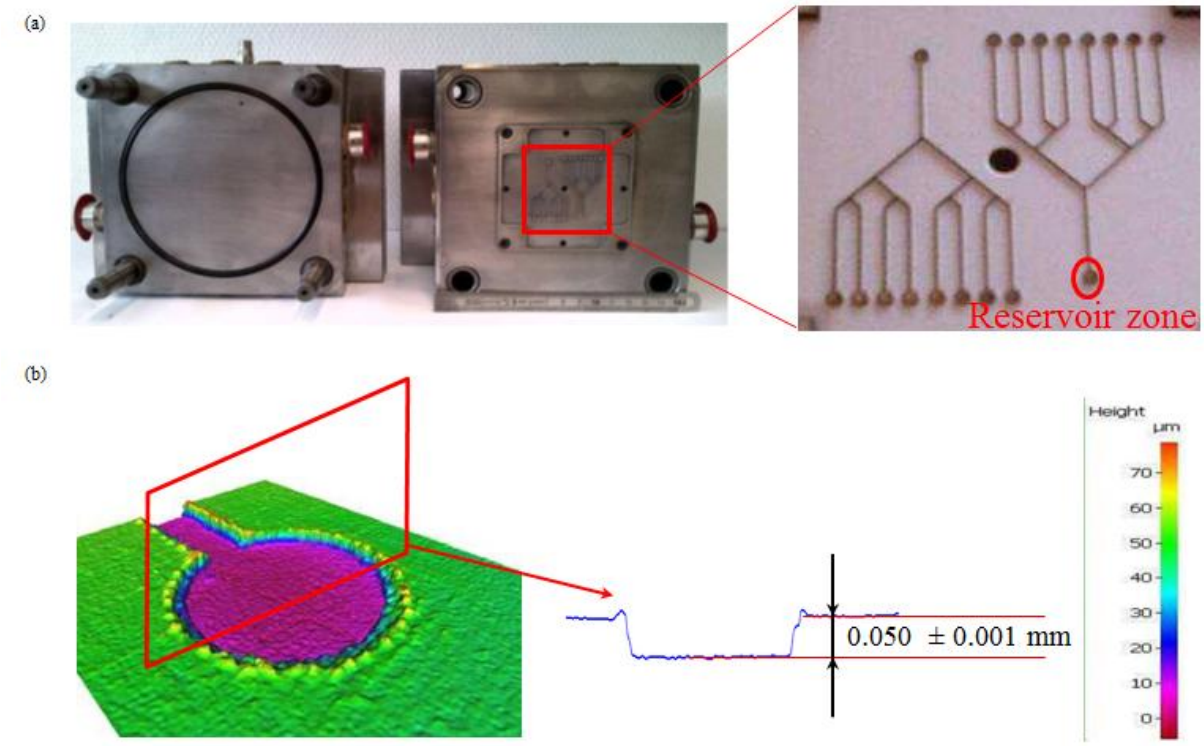

Fig. 13. (a) Microfluidic mould die features with associated reservoir zone corresponding to the numerical geometry model (b) The reservoir zone of the replicated PMMA microfluidic mould with a detailed cross-sectional profile.

Table

Nomenclature

A, n_2	Norton constants
D	Final diameter
D_0	Initial diameter
d	Mould displacement
d_{max}	Maximum mould displacement
E	Elastic modulus
F^c	Compressive force
f	Proportion of elasticity in the viscoelastic branch to total elasticity
H	Final height
H_0	Initial height
H'	Power law hardening
K	Total elastic modulus
K_p	Elastic modulus in the elastoplastic branch
K_v	Elastic modulus in the viscoelastic branch
m	Time-hardening power law parameter
n_1	Work hardening exponent
$PMMA$	Poly-methyl methacrylate
S	Final cross-sectional area
S_0	Initial cross-sectional area
T_g	Glass transition temperature
t	Testing time
$\dot{\varepsilon}$	Strain rate
ε_v^{el}	Elastic strain of the viscoelastic branch
ε_p^{el}	Elastic strain in the elastoplastic branch
ε^{el}	Total elastic strain
ε^{pl}	Plastic strain
ε^{v}	Viscous strain
ε	Total strain
η	Viscosity
σ	Total stress
σ_p	Plastic stress
σ_γ	Initial yield stress
σ_v	Viscous stress
ϑ	Displacement rate
υ	Poisson's ratio

Table 1. Two-layer viscoplastic model parameters of PMMA at $T_g + 20$ °C.

Parameter	Value
K_p (MPa)	3.61
K (MPa)	33.38
f	0.89
A (Pa)$^{-n_2}$	6.63×10^{-6}
n_2	0.88
m	0
v	0.4

Table 2. Plastic strain of PMMA at $T_g + 20$ °C.

σ (MPa)	ε^{pl}
0.5 ± 0.0001	0 ± 0.0005
0.8 ± 0.0001	0.01 ± 0.0005
1.1 ± 0.0001	0.04 ± 0.0005
1.4 ± 0.0001	0.08 ± 0.0005

Table 3. Cavity filling ratio versus different imposed displacements and constitutive behaviours.

Imposed displacement (mm)	Filling ratio		
	Elastic	Elastoplastic	Elastic-viscoplastic
0.05	43.00%	46.00%	98.40%
0.10	88.00%	91.25%	98.90%
0.15	91.50%	95.00%	99.16%
0.20	95.34%	97.00%	99.99%

Declaration of interests

☒ The authors declare that they have no known competing financial interests or personal relationships that could have appeared to influence the work reported in this paper.

☐The authors declare the following financial interests/personal relationships which may be considered as potential competing interests:
